Journal of Asian Earth Sciences 36 (2009) 168–182

Contents lists available at ScienceDirect

Journal of Asian Earth Sciences

journal homepage: www.elsevier.com/locate/jseaes

U–Pb zircon, geochemical and Sr–Nd–Hf isotopic constraints on the age and origin of Early Palaeozoic I-type granite from the Tengchong–Baoshan Block, Western Yunnan Province, SW China

Shen Liu [a,b,c,d,*], RuiZhong Hu [a], Shan Gao [c], CaiXia Feng [a], Zhilong Huang [a], Shaocong Lai [b], Honglin Yuan [b], Xiaoming Liu [b], Ian M. Coulson [d], Guangying Feng [a], Tao Wang [a], YouQiang Qi [a]

[a] State Key Laboratory of Ore Deposit Geochemistry, Institute of Geochemistry, Chinese Academy of Sciences, Guiyang 550002, China
[b] State Key Laboratory of Continental Dynamics, Northwest University, Xi'an 710069, China
[c] State Key Laboratory of Geological Processes and Mineral Resources, China University of Geosciences, Wuhan 430074, China
[d] Solid Earth Studies Laboratory, Department of Geology, University of Regina, Regina, Saskatchewan S4S 0A2, Canada

ARTICLE INFO

Article history:
Received 20 November 2008
Received in revised form 29 April 2009
Accepted 16 May 2009

Keywords:
Granite
U–Pb zircon age
Geochemistry
Sr–Nd–Hf isotopes
Early Palaeozoic
Western Yunnan Province

ABSTRACT

Herein we present new U–Pb zircon ages, whole-rock geochemical data and Nd–Sr–Hf isotopic data for an Early Palaeozoic monzogranite batholith from the Tengchong–Baoshan Block, Western Yunnan Province, China. Mineralogical and geochemical features suggest that this granitoid is a high-K, calc-alkaline, I-type granite. SHRIMP and laser ablation ICP-MS (LA-ICP-MS) analysis of zircon yields ages of between 499 ± 5 Ma and 502 ± 5 Ma, for three samples from the batholith. The monzogranite is characterised by high initial $^{87}Sr/^{86}Sr$ (0.7132–0.7144), negative $\varepsilon_{Nd}(t)$ (−9.7 to −9.40) and $\varepsilon_{Hf}(t)$ (−10 to −13.1), and is interpreted to derive from remelting of pre-existing Palaeoproterozoic, high-K, metabasaltic rocks of the upper crust. The granitoid magma underwent extensive fractional crystallisation of biotite ± hornblende, ilmenite, titanite, K-feldspar and plagioclase during emplacement. The crystallisation temperature of the magma lies in the range 633–733 °C, however, there is no evidence to suggest crustal assimilation occurred during its ascent. Like the ~500 Ma, I-type granite of this study, there occur numerous granitoid rocks of Early Palaeozoic age (490–470 Ma) in adjacent regions across the entire Tengchong–Baoshan Block (Chen et al., 2004, 2005; Song et al., 2007). This episode of plutonism is coeval with the widespread granitoid magmatism found throughout the Indian Plate and the Himalayan Orogenic Belt that are both subordinate parts of the ancient, Gondwana supercontinent. We infer, therefore, that the Tengchong–Baoshan Block may also have formed part of Gondwana, and that it separated from this supercontinent along with other crustal blocks during the Late Palaeozoic. Moreover, based on the findings of this study, we document the occurrence of arc-related magmatism in the Tengchong–Baoshan Block during the late Palaeoproterozoic.

1. Introduction

The geological evolution of SE Asia during the Palaeozoic to Mesozoic can be regarded as an accretion history resulting from the amalgamation of several micro-continents or continental blocks into the Eurasian continent, related to the closure of the Tethys Ocean (Sengör, 1984; Sengör et al., 1993; Metcalfe, 1996; Wopfner, 1996; Ueno, 2000). The Western Yunnan Province (SW China) is one of the more important branches of the eastern Tethyan tectonic belt, and therefore bears significance for the development of the Tethyan belt within Southeast (SE) Asia (Chen et al., 2004, 2005, 2006). The Western Yunnan is composed of several continental blocks separated by tectonic sutures (Chen et al., 2004). In this paper we focus on the Simao and the Tengchong–Baoshan blocks (Fig. 1a). The Tengchong–Baoshan Block comprises both the Tengchong and Baoshan blocks, and the Luxi geosyncline (Chen et al., 2005). However, the tectonic environment to which the Tengchong–Baoshan Block belongs is controversial. For example, on the basis of palaeontological evidence, Wang (1984) suggested that the Tengchong–Baoshan Block is a part of the former Gondwana supercontinent. By contrast, Fang et al. (1990) suggested that there is no affinity between the Tengchong–Baoshan Block and Gondwana due to their different Palaeozoic stratum sequences and fossil groups. More recently, based upon tectonic and geophysical evidence, the Tengchong–Baoshan Block has again

* Corresponding author. Address: State Key Laboratory of Ore Deposit Geochemistry, Institute of Geochemistry, Chinese Academy of Sciences, Guiyang 550002, China. Tel.: +86 851 5895187; fax: +86 851 5891664.
E-mail address: liushen@vip.gyig.ac.cn (S. Liu).

1367-9120/$ - see front matter © 2009 Elsevier Ltd. All rights reserved.
doi:10.1016/j.jseaes.2009.05.004

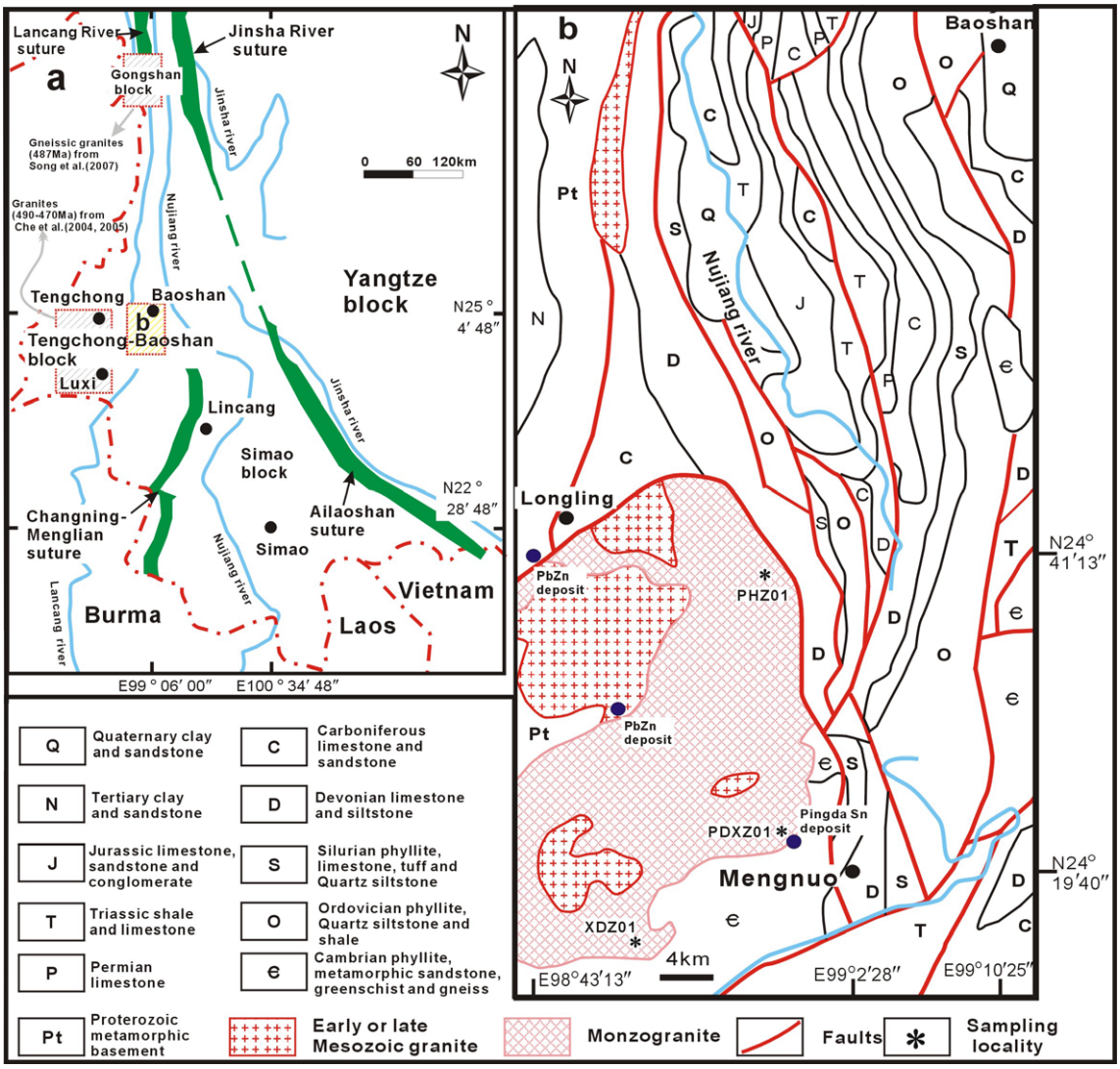

Fig. 1. (a) Simplified tectonic map of Western Yunnan Province, China (modified from Chen et al., 2004). (b) The geological map of the Tengchong–Baoshan Block and the sampling localities for the granites.

been considered as a micro-segment of the ancient supercontinent, Gondwana (e.g., Fang and Fan, 1993; Metcalfe, 1996; Wopfner, 1996; Zhong, 1998; Pan et al., 2004).

Early Palaeozoic granitoids are widely distributed throughout the Tengchong–Baoshan (Chen et al., 2004, 2005) and the Gongshan blocks (Song et al., 2007) (Fig. 1a), and investigation of these granitoids can help in understanding the provenance and tectonic environment of these two areas. For example, the 490–470 Ma granitoids of both the Tengchong–Baoshan Block and the Gongshan Block (Chen et al., 2004, 2005; Song et al., 2007) represent magmatic activity that occurred during the post-Pan-African movement. Moreover, these magmatic events imply a comparable history for basement outcrop during the Early Palaeozoic between SE Asia and the Western Tethyan region. Basement outcrops in the Alpine belt and probably also in the European Variscides (Von Raumer et al., 2002) are considered as continental blocks, having fragmented from Gondwana prior to or simultaneously with those occurring in SE Asia. Accordingly, in order to verify whether or not the Tengchong–Baoshan Block pertains to Gondwana, systematic studies of all the Early Palaeozoic igneous rocks present therein, are required. As such, in this study we have selected granitoid rocks from those distributed across the Tengchong–Baoshan Block in the Western Yunnan Province to carry out a detailed geochronological and geochemical investigation. We present new SHRIMP and laser ablation ICP-MS (LA-ICP-MS) zircon U–Pb ages, as well as rock petrography, whole-rock geochemistry, and Sr–Nd–Hf isotopic data, for the granites. Our aim was to: (1) constrain the emplacement age(s) of the granitoids; (2) decipher their petrogenesis and tectonic significance, and (3) understand the tectonic evolution of Western Yunnan, and its relationship to the Gondwana supercontinent.

2. Geological setting and petrography

The Tethyan belt in Western Yunnan Province is an important crustal feature, consisting of several micro-continental blocks and tectonic belts (e.g., the Tengchong–Baoshan lock, Simao Block, Gongshan Block, Gaoligong orogenic belt and Changning–Menglian suture zone; Wu et al., 1995; Wang, 1996; Zhang et al., 1997; Zhong, 1998) (Fig. 1a). Folding and faulting are abundant within the Tengchong–Baoshan Block and our study area is located between Longling and Mengnuo, in the southwestern corner of this block (Fig. 1b). To the west of the Nujiang River, emplacement of granitoid rocks that comprise a batholith was primarily fault-con-

trolled; the total exposed area of these granitoids is estimated at ca. 800 km^2 (Fig. 1b). The batholith intruded Neoproterozoic to Cambrian low-grade metamorphic, terrestrial, sedimentary rocks, and was in turn intruded by some smaller granite intrusions, referred to as the early or late Mesozoic granite (126–118 Ma; Yang et al., 2006). The studied granitoids are neither deformed nor metamorphosed. At the southeastern corner of the batholith, occurs the Pingda stannum (Sn) deposit, while within the western and northwestern margins, two Pb–Zn deposits have been identified (Fig. 1b).

Monzogranite is the dominant rock type, comprising more than 95% of the batholith; granodiorite is subordinate. Samples collected for this study are all of monzogranite; they contain 25–40% quartz, 15–28% K-feldspar, 30–47% plagioclase (An_{20-38}), 2–8% biotite, 0–5% hornblende and minor (<1%) muscovite. Accessory minerals include zircon, apatite, allanite, titanite, magnetite and ilmenite.

3. Analytical techniques

3.1. SHRIMP and LA-ICP-MS zircon U–Pb methods

Zircon was separated from three ~4 kg samples (PDXZ01, XDZ01 and PHZ01) taken from various sampling locations within the batholith (Fig. 1b), using conventional heavy liquid and magnetic techniques. Representative zircon grains were handpicked under a binocular microscope, mounted in epoxy resin, and then polished and coated with gold. Zircons were documented with transmission and reflecting light microscopy as well as under cathodoluminescence (CL) imagery to reveal their internal make-up (Fig. 2). U–Pb isotopic analysis for PDXZ01 and XDZ01 were undertaken using the Sensitive High-Resolution Ion Microprobe (SHRIMP-II) at the Chinese Academy of Geological Sciences (Beijing) (Table 1). Procedures have been described in detail by Compston et al. (1992), Williams (1998) and Song et al. (2002). Single crystals were dated without air abrasion. The U–Pb isotope data were collected in sets of five scans throughout the masses, and a reference zircon, TEM (417 Ma), was analysed after every four unknown zircons. The uncertainties in ages are cited as 1σ, and the weighted mean ages are quoted at the 95% confidence level (2σ).

Laser ablation techniques were used for an additional age determination (Table 2). The U–Pb isotopic analyses for sample PHZ01 were obtained with an Elan 6100 DRC ICP-MS equipped with 193 nm Excimer lasers, housed at the Department of Geology, Northwest University, Xi'an, China. Zircon 91500 was used as a standard and NIST 610 was used to optimise the machine. A mean age of 1062 Ma was obtained for the 91500 zircon standard. The spot diameter was 30 μm. Corrections for common-Pb were made using the method of Andersen (2002). Data were processed using the GLITTER and ISOPLOT (Ludwig, 2003) programs. Errors on individual analyses by LA-ICP-MS are quoted at the 95% (1σ) confidence level. The details of the analytical procedures have been described by Yuan et al. (2004).

3.2. Major, trace elemental and isotopic analysis

Nineteen samples were collected for major and trace element analysis and ten samples were chose for Sr–Nd–Pb isotopic study. Whole-rock samples were trimmed to remove weathered surfaces, cleaned with deionized water, crushed and then powdered with an agate mill.

Major oxides were analysed with a PANalytical Axios-advance X-ray fluorescence spectrometer (XRF) at the State Key Laboratory of Ore Deposit Geochemistry, Institute of Geochemistry, Chinese Academy of Science (IGCAS). Fused glass discs were used and the analytical precision, as determined on the Chinese National standard GSR-1, was better than 5% (Table 3). Loss on ignition (LOI) was obtained using 1 g of powder heated to 1100 °C for 1 h.

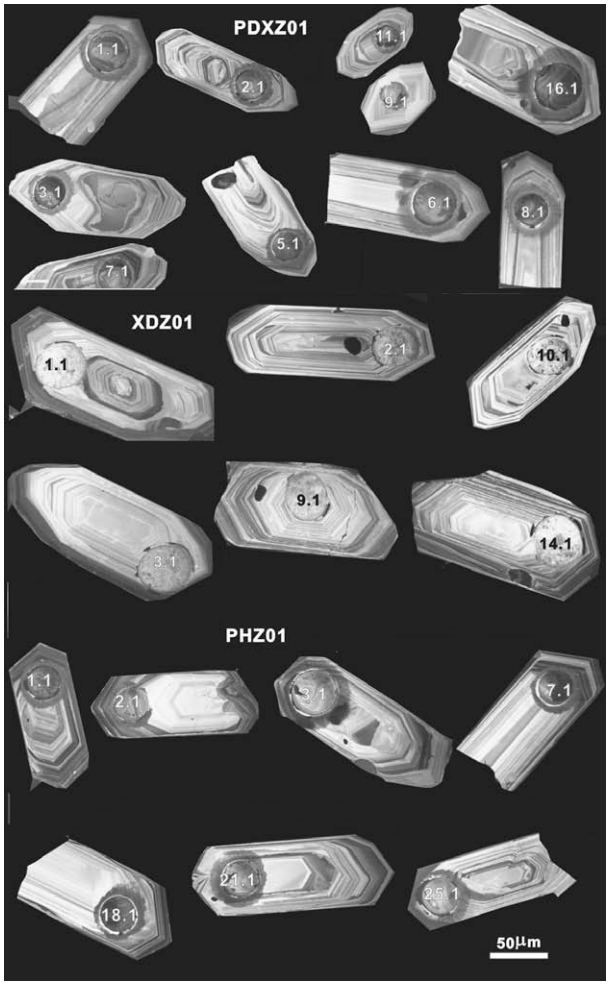

Fig. 2. Representative cathodoluminescence images of zircon grains from the monzogranite samples (PDXZ01, XDZ01 and PHZ01). The numbers correspond to the spot analyses given in Table 1.

Trace elements were analysed with a plasma optical emission mass spectrometer (POEMS) ICP-MS system at the National Research Center of Geoanalysis, Chinese Academy of Geosciences in Beijing. A detailed account of the analytical procedures has been given by Qi et al. (2000). The discrepancy between triplicates is less than 5% for all elements, while the analysis of international standards, OU-6 and GBPG-1, are in agreement with recommended values (Table 4).

For Rb–Sr and Sm–Nd isotope analysis, sample powders were spiked with mixed isotope tracers, dissolved in Teflon capsules with HF + HNO_3 acid, and separated by conventional cation-exchange technique (Zhang et al., 2001). Isotopic measurement was performed on the MAT-262 TIMS at the Institute of Geology and Geophysics, the Chinese Academy of Sciences (IGGCAS) in Beijing. Procedural blanks were <100 pg for Sm and Nd and <500 pg for Rb and Sr. The mass fractionation corrections for the Sr and Nd isotopic ratios were based on $^{86}Sr/^{88}Sr = 0.1194$ and $^{146}Nd/^{144}Nd = 0.7219$, respectively. The analyses of standards during the period of analysis were as follows: NBS987 gave $^{87}Sr/^{86}Sr = 0.710245 \pm 14$ (2σ); La Jolla gave $^{143}Nd/^{144}Nd = 0.511861 \pm 9$ (2σ).

Table 1
SHRIMP U–Pb isotopic data for PDXZO1 and XDZO1 from the granites in Western Yunnan Province.

Spot	$^{206}Pbc(\%)$	U (ppm)	Th (ppm)	$^{232}Th/^{23}U$	$^{206}Pb^{*}$ (ppm)	$^{206}Pb/^{238}U$(Ma)	$^{207}Pb^{*}/^{206}Pb^{*}$	±%	$^{207}Pb^{*}/^{235}U$	±%	$^{206}Pb^{*}/^{238}U$	±%
PDXZ01												
1.1	1.03	275	131	0.49	19.0	493.7 ± 9.0	0.0555	5.3	0.609	5.6	0.0796	1.9
2.1	0.18	1947	745	0.40	139	512.3 ± 8.1	0.0560	1.8	0.639	2.4	0.0827	1.6
3.1	1.62	323	154	0.49	22.4	493.6 ± 9.0	0.0522	7.7	0.573	7.9	0.0796	1.9
4.1	1.72	255	106	0.43	17.4	484.0 ± 10.0	0.0532	9.8	0.572	10	0.0780	2.4
5.1	1.35	220	86	0.40	15.0	485.8 ± 9.4	0.0527	8.7	0.569	8.9	0.0783	2.0
6.1	0.28	761	305	0.41	52.6	498.0 ± 8.2	0.0580	1.4	0.643	2.2	0.0803	1.7
7.1	0.24	1188	553	0.48	85.7	518.5 ± 9.1	0.0561	2.8	0.648	3.3	0.0838	1.8
8.1	0.25	1802	982	0.56	126	501.8 ± 8.0	0.0565	1.3	0.631	2.1	0.0810	1.6
9.1	0.82	304	170	0.58	21.0	494.5 ± 8.4	0.0583	7.9	0.640	8.1	0.0797	2.0
10.1	0.53	221	103	0.48	56.0	1661 ± 23	0.1486	1.2	6.020	2.3	0.2940	1.9
11.1	1.14	450	213	0.49	32.2	510 ± 11.0	0.0532	5.4	0.603	5.8	0.0822	2.2
12.1	1.18	600	269	0.46	41.7	496.6 ± 8.8	0.0520	7.9	0.574	8.1	0.0801	1.8
13.1	0.92	887	217	0.25	64.8	521.0 ± 9.7	0.0515	3.8	0.598	4.3	0.0842	2.1
14.1	1.25	297	130	0.45	20.2	484.9 ± 9.4	0.0574	8.2	0.618	8.4	0.0781	2.0
15.1	0.46	342	135	0.41	24.0	504.5 ± 9.7	0.0589	5	0.661	5.4	0.0814	2.0
16.1	0.88	238	112	0.49	16.2	487.5 ± 9.1	0.0603	4.6	0.653	5	0.0786	1.9
17.1	0.75	628	205	0.34	42.9	490.3 ± 8.2	0.0534	3.4	0.582	3.8	0.0790	1.7
XDZ01												
1.1	0.50	627	243	0.40	43.2	495.2 ± 8.3	0.0557	3.2	0.613	3.7	0.0798	1.7
2.1	0.90	420	143	0.35	29.1	495.6 ± 8.7	0.0552	4.9	0.608	5.2	0.0799	1.8
3.1	0.21	1132	350	0.32	76.8	489.1 ± 7.9	0.0563	1.8	0.611	2.5	0.0788	1.7
4.1	0.48	670	251	0.39	47.8	511.7 ± 8.5	0.0561	3.1	0.639	3.6	0.0826	1.7
5.1	0.47	676	334	0.51	47	500.0 ± 9.4	0.057	4.3	0.634	4.8	0.0807	2
6.1	0.53	1003	514	0.53	72.3	516.7 ± 8.4	0.0547	2.8	0.629	3.3	0.0834	1.7
7.1	0.54	859	374	0.45	60.4	504.2 ± 8.3	0.055	2.9	0.617	3.4	0.0814	1.7
8.1	0.49	1054	486	0.48	73.7	501.6 ± 8.1	0.0552	2.4	0.616	2.9	0.0809	1.7
9.1	0.21	1554	195	0.13	109.9	509.2 ± 9.3	0.0554	1.3	0.628	2.3	0.0822	1.9
10.1	0.05	3095	1084	0.36	222.1	516.9 ± 8.1	0.0563	0.8	0.648	1.8	0.0835	1.6
11.1	0.71	220	110	0.52	14.9	485.1 ± 9.1	0.0576	6.2	0.620	6.5	0.078∼1	1.9
12.1	0.21	721	367	0.53	49.4	493.6 ± 8.1	0.058	1.54	0.637	2.3	0.0796	1.71
13.1	0.18	1468	485	0.34	105.6	517.7 ± 8.2	0.0567	1.2	0.654	2.1	0.0836	1.7
14.1	0.06	1064	339	0.33	74.8	506.7 ± 8.7	0.0575	2.2	0.648	2.8	0.0818	1.8

(1) Errors are 1σ; Pb_c and Pb^{*} indicate the common and radiogenic portions, respectively.
(2) Error in standard calibration was 1.29% (not included in above errors but required when comparing data from different mounts).
(3) Common Pb corrected using measured ^{204}Pb.

Table 2
Laser ablation ICP-MS U–Pb data of PHZO1 from the granites from Western Yunnan Province.

Isotopic ratios											Age (Ma)					
Spot	U (ppm)	Th (ppm)	Pb (ppm)	$^{238}U/^{232}Th$	$^{207}Pb/^{206}Pb$	1σ	$^{207}Pb/^{235}U$	1σ	$^{206}Pb/^{238}U$	1σ	$^{207}Pb/^{206}Pb$	1σ	$^{207}Pb/^{235}U$	1σ	$^{206}Pb/^{238}U$	1σ
1	319	124	30.8	2.57	0.0541	0.0009	0.60187	0.0085	0.08077	0.0005	374	20	478	5	501	3
2	288	101	27.7	2.86	0.0562	0.0011	0.62817	0.0106	0.08111	0.0006	459	25	495	7	503	3
3	450	129	42.6	3.49	0.0558	0.0009	0.62678	0.008	0.08147	0.0005	445	17	494	5	505	3
4	518	192	50.0	2.69	0.0550	0.0009	0.61426	0.008	0.08099	0.0005	413	17	486	5	502	3
5	203	122	20.0	1.66	0.0532	0.0011	0.57429	0.0108	0.07834	0.0006	336	29	461	7	486	3
6	273	151	27.8	1.81	0.0576	0.0014	0.64593	0.015	0.08135	0.0007	515	36	506	9	504	4
7	696	158	65.1	4.41	0.0567	0.0007	0.64295	0.0064	0.08224	0.0005	480	12	504	4	509	3
8	184	104	18.9	1.78	0.0562	0.0013	0.63577	0.0132	0.08211	0.0006	459	32	500	8	509	4
9	563	273	56.9	2.06	0.0551	0.0008	0.62401	0.0077	0.08216	0.0005	416	16	492	5	509	3
10	487	165	46.2	2.96	0.0560	0.0009	0.62313	0.0079	0.08067	0.0005	454	17	492	5	500	3
11	163	116	15.6	1.40	0.0557	0.0014	0.55648	0.0128	0.07242	0.0006	442	36	449	8	451	4
12	376	172	37.4	2.19	0.0569	0.0009	0.63871	0.009	0.08148	0.0006	486	19	502	6	505	3
13	545	251	54.1	2.17	0.0555	0.0008	0.62484	0.0076	0.08173	0.0005	431	16	493	5	506	3
14	1402	373	127	3.76	0.0552	0.0007	0.59485	0.0061	0.07811	0.0005	422	12	474	4	485	3
15	255	119	25.6	2.15	0.0556	0.001	0.62664	0.0097	0.08171	0.0006	438	22	494	6	506	3
16	1747	650	162	2.69	0.0560	0.0007	0.59969	0.005	0.07768	0.0005	452	9	477	3	482	3
17	601	165	57.0	3.63	0.0566	0.0009	0.63676	0.0084	0.08163	0.0005	475	18	500	5	506	3
18	924	208	79.1	4.45	0.0564	0.0008	0.57878	0.0074	0.07446	0.0005	467	32	464	5	463	3
19	458	134	43.2	3.42	0.0536	0.001	0.60383	0.0105	0.08171	0.0006	355	26	480	7	506	4
20	119	83	12.5	1.44	0.0578	0.0021	0.64693	0.0223	0.0812	0.0009	522	57	507	14	503	5
21	299	164	31.3	1.82	0.0554	0.0011	0.63608	0.0109	0.08334	0.0006	427	25	500	7	516	4
22	351	82	31.6	4.29	0.0565	0.0011	0.61036	0.0109	0.0783	0.0006	474	27	484	7	486	3
23	223	122	26.9	1.82	0.0555	0.0012	0.73855	0.0151	0.0965	0.0008	433	32	562	9	594	4
24	488	245	49.4	1.99	0.0554	0.0009	0.62687	0.0084	0.08205	0.0005	430	18	494	5	508	3
25	166	102	17.1	1.62	0.0561	0.0014	0.62534	0.0139	0.08086	0.0007	456	35	493	9	501	4
26	2170	293	198	7.39	0.0553	0.0006	0.62677	0.0047	0.08223	0.0005	424	8	494	3	509	3
27	1438	338	131	4.25	0.0557	0.0007	0.61019	0.0061	0.07947	0.0005	440	12	484	4	493	3
28	611	181	57.1	3.38	0.0549	0.0008	0.58558	0.0066	0.07736	0.0005	409	14	468	4	480	3

Th and U contents are given directly, Pb = $^{204}Pb * 0.014 + ^{206}Pb * 0.241 + ^{207}Pb * 0.221 + ^{208}Pb * 0.524$.

Table 3
Major oxides (wt.%) of the granites from Western Yunnan Province.

Sample	PH5-7	PH5-6	PH5-4	PH5-3	PH4-7	PH4-6	PH4-5	PH4-4	PH3-7	PH3-4	PH3-2	PH3-1	XD6	XD4	XD1	PDX16	PDX6	PDX5	PDX4	PDX3	GSR-1 RV*	GSR-1 MV*
Rock type	Monzogranite	Monzogranite	Monzogranite	Monzogranite	Monzogranite	Monzogranite	Monzogranite	Monzogranite	Monzogranite	Monzogranite	Monzogranite	Monzogranite	Monzogranite	Monzogranite	Monzogranite	Monzogranite	Monzogranite	Monzogranite	Monzogranite	Monzogranite	granite	granite
SiO_2	71.13	69.81	65.92	65.85	71.93	71.81	72.03	71.88	68.52	68.88	68.63	66.16	68.46	69.35	72.98	63.86	66.59	64.30	65.83	64.99	72.83	72.65
TiO_2	0.27	0.35	0.40	0.42	0.29	0.31	0.31	0.33	0.48	0.36	0.42	0.53	0.44	0.42	0.23	0.65	0.46	0.67	0.60	0.53	0.29	0.29
Al_2O_3	14.60	14.66	15.26	15.47	13.94	13.99	14.39	14.02	15.17	15.23	15.43	15.69	15.43	14.98	13.67	15.93	15.46	14.62	15.55	16.53	13.40	13.52
Fe_2O_3	2.86	3.34	4.56	4.39	2.99	3.22	3.16	3.38	4.39	3.57	3.91	4.82	4.11	3.98	2.35	6.04	4.44	6.93	5.68	5.20	2.14	2.18
MnO	0.09	0.07	0.08	0.08	0.08	0.10	0.10	0.10	0.10	0.10	0.09	0.10	0.09	0.10	0.07	0.13	0.11	0.17	0.13	0.12	0.06	0.06
MgO	0.87	1.89	1.52	1.58	0.73	0.79	0.77	0.85	1.28	1.06	1.06	1.33	1.25	1.22	0.61	2.22	1.51	2.25	2.31	1.75	0.42	0.46
CaO	2.41	1.22	3.54	3.41	2.21	2.47	2.20	2.31	3.29	2.77	3.07	3.43	3.40	3.09	1.97	4.11	4.24	3.82	4.12	4.20	1.55	1.56
Na_2O	3.01	2.93	3.22	3.15	3.26	3.27	3.29	3.28	3.17	3.07	3.24	3.17	3.12	3.03	3.65	2.99	3.02	2.87	2.57	2.54	3.13	3.15
K_2O	4.42	3.59	4.31	4.52	3.62	3.31	3.53	3.32	3.30	3.78	3.27	3.29	3.15	3.29	3.69	3.13	3.40	3.15	3.39	3.23	5.01	5.03
P_2O_5	0.09	0.11	0.12	0.13	0.10	0.10	0.10	0.10	0.14	0.11	0.12	0.15	0.12	0.12	0.09	0.15	0.11	0.16	0.14	0.13	0.09	0.11
LOI	0.48	1.44	0.60	0.66	0.47	0.55	0.57	0.57	0.42	0.73	0.52	0.53	0.40	0.59	0.38	0.61	1.26	0.78	0.28	0.84	0.70	0.69
Total	100.23	99.42	99.53	99.65	99.60	99.93	100.45	100.15	100.25	99.66	99.76	99.20	99.98	100.16	99.69	99.82	100.60	99.71	100.60	100.05	99.62	99.7
Na_2O/K_2O	0.68	0.82	0.75	0.70	0.90	0.99	0.93	0.99	0.96	0.81	0.99	0.96	0.99	0.92	0.99	0.96	0.89	0.91	0.76	0.79		
T (°C)	633	668	710	733	661	658	673	667	646	650	659	663	643	652	635	688	673	683	674	682		
A/CNK	1.22	1.49	1.16	1.17	1.24	1.25	1.28	1.26	1.29	1.31	1.32	1.32	1.33	1.32	1.16	1.32	1.24	1.26	1.34	1.44		
A/NK	1.50	1.68	1.53	1.54	1.50	1.56	1.56	1.56	1.73	1.67	1.74	1.79	1.81	1.75	1.37	1.92	1.79	1.80	1.97	2.15		

LOI = loss on ignition. RV*: recommended values; MV*: measured values; the values for GSR-1 from Govindaraju (1994).
A/CNK = $(2 * Al_2O_3/101.96)/(CaO/56.08+2 * Na_2O/61.98+2 * K_2O/94.2)$; A/NK=$(2 * Al_2O_3/101.96)/(2 * Na_2O/61.98 + 2 * K_2O/94.2)$.

3.3. In situ zircon Hf isotopic analysis

In situ zircon Hf isotopic analysis was conducted using a Neptune Multicollector-ICP-MS, equipped with a 193 nm laser, at the Institute of Geology and Geophysics, the Chinese Academy of Sciences in Beijing, China. During the analyses, a laser repetition rate of 10 Hz at 100 mJ was used and the spot sizes were 32 and 63 μm. The raw count rates for ^{172}Yb, ^{173}Yb, ^{175}Lu, $^{176}(Hf + Yb + Lu)$, ^{177}Hf, ^{178}Hf, ^{179}Hf, ^{180}Hf and ^{182}W were collected and the isobaric interference corrections for ^{176}Lu and ^{176}Yb on ^{176}Hf, precisely determined. ^{176}Lu was calibrated using the ^{175}Lu value and the correction was applied to ^{176}Hf. The $^{176}Yb/^{172}Yb$ value of 0.5887 and mean β_{Yb} value obtained during Hf analysis on the same spot were applied for the interference correction of ^{176}Yb on ^{176}Hf (Lizuka and Hirata, 2005). The detailed analytical technique for this method was described in Xu et al. (2004) and Wu et al. (2006). During the analysis, $^{176}Hf/^{177}Hf$ and $^{176}Lu/^{177}Hf$ ratios for the standard zircon (91500) were 0.282300 ± 30 ($2\sigma_n$, $n = 24$) and 0.00030, similar to the commonly accepted $^{176}Hf/^{177}Hf$ ratio of 0.282302 ± 8 and 0.282306 ± 8 (2σ), determined using the solution method (Goolaerts et al., 2004; Woodhead et al., 2004).

4. Results

4.1. Zircon U–Pb age

Zircon is abundant in the studied monzogranite samples. Zircons from PDXZ01, XDZ01 and PHZ01 are euhedral and range up to 100 μm in size; most of them are transparent to light brown in colour, and exhibit magmatic oscillatory zoning (Fig. 2). Seventeen grains were analysed from sample PDXZ01, of which sixteen may be pooled to yield a weighted mean $^{206}Pb/^{238}U$ age of 498.5 ± 4.6 Ma (2σ) (MSWD = 1.6; Table 1 and Fig. 3a). Analysis 10.1 gave a much older age of 1661 Ma. This is interpreted to be an inherited zircon. Fourteen grains from sample XDZ01 gave a weighted mean age of 502 ± 4.7 Ma (2σ) (MSWD = 1.18; Table 1 and Fig. 3b). LA-ICP-MS data on 25 grains from sample PHZ01 yielded a weighted mean age of 500.1 ± 4.1 Ma (1σ) (MSWD = 1.7; Table 2 and Fig. 3c). Analytical uncertainties result in some ages less than 490 Ma and one analysis with an age of 594 Ma (spot 23). In summary, the U–Pb data indicate that the monzogranite crystallised at ca. 500 Ma and that it contains a minor component of inherited zircon with both Palaeoproterozoic (1661 Ma) and Neoproterozoic (594 Ma) ages.

4.2. Major and trace elements

Whole-rock major and trace element data for the monzogranite samples are listed in Tables 3 and 4. The monzogranite exhibits a wide range in chemical composition, with SiO_2 ranging from 64.3% to 72.98%, CaO, 1.2–4.2%, Fe_2O_3, 2.35–6.93%, and MgO, 0.61–2.31%. These rocks have high K_2O (3.13–4.52%) and Al_2O_3 (13.67–16.53%), moderate Na_2O (2.54–3.65%) contents and low Na_2O/K_2O (<1). All of the samples fall within both the subalkaline field, on the total alkali-silica (TAS) diagram (Fig. 4a) and the high-K calc-alkaline series, on the K_2O *vs.* SiO_2 diagram (Fig. 4b). In a plot constructed in terms of the molar ratios of Al/(Na + K) (A/NK) and Al/(Ca + Na + K) (A/CNK or alumina saturation index), all samples are peraluminous and fall within the field of S-type other than I-type granites due to their high A/CNK ratios (1.16–1.49) (Fig. 4c), according to the criteria of Chappell and White (1992). With increasing SiO_2, Al_2O_3, Fe_2O_3, MgO, CaO, TiO_2, P_2O_5, Sr, Ba and Zr all decrease, whereas K_2O rises; Na_2O and Rb remain nearly constant (Figs. 5 and 6). These chemical variations are con-

Table 4
Major oxides (wt.%) of the granites from Western Yunnan Province.

Sample	PH5-7	PH5-6	PH5-4	PH5-3	PH4-7	PH4-6	PH4-5	PH4-4	PH3-7	PH3-4	PH3-2	PH3-1	XD6	XD4	XD1	PDX16	PDX6	PDX5	PDX4	PDX3	GBPG-1(RV*)	GBPG-1(MV*)	OU-6(RV*)	OU-6(MV*)
Ba	747	552	511	447	585	457	542	476	1130	695	676	815	732	785	333	802	580	787	745	745	908	921	479	486
Rb	169	184	245	246	177	160	162	164	140	162	157	164	149	158	164	150	104	190	139	135	56.2	61.4	120	122
Sr	117	86	84.8	74.1	125	116	123	119	173	125	161	177	152	137	67	178	194	184	192	212	364	377	131	136
Ta	1.05	1.42	2.10	1.98	1.40	1.49	1.33	1.50	0.93	1.20	1.16	1.12	1.03	1.08	1.30	1.13	0.83	1.10	1.12	0.99	0.40	0.46	1.06	1.02
Nb	7.37	11.3	11.9	12.2	9.68	10.0	9.89	10.4	11.4	9.22	9.92	12.8	9.88	9.78	10.3	11.1	7.72	11.2	9.92	8.92	9.93	8.74	14.8	15.3
Hf	0.53	0.85	1.54	1.94	0.80	0.86	1.04	0.95	0.59	0.67	0.74	0.77	0.58	0.66	0.63	1.46	1.02	1.27	1.17	1.29	6.07	5.93	4.70	4.86
Zr	12.5	18.3	25.8	27.3	18.9	18.1	21.9	20.3	15.7	16.3	18.5	20.8	14.9	16.7	12.4	31.2	24.3	29.2	26.0	28.2	232	228	174	183
Y	21.0	22.2	22.8	23.1	25.0	31.3	29.6	30.2	18.6	25.6	18.6	24.3	22.1	24.1	15.5	27.0	15.7	26.0	22.0	18.9	18.0	17.2	27.4	26.2
Sc	6 39	8.90	5.82	5.02	8.94	7.69	7.89	8.64	10.8	8.74	9.43	12.0	9.68	9.39	4.98	14.7	8.34	15.2	12.1	9.85	13.9	13.9	22.1	21.8
V	32.8	46.3	20.3	19.4	34.4	37.2	35.2	37.7	57.3	46.9	50.4	67.8	56.7	53.9	24.7	103.2	68.0	107	89.9	78.9	96.5	103	129	131
Cr	20.6	26.7	13.6	21.3	13.6	82.0	60.2	20.1	92.5	35.6	21.7	18.7	26.2	35.0	14.9	30.4	33.7	40.1	30.9	25.9	181	187	70.8	73.5
Co	4.75	4.88	3.50	3.33	4.25	4.80	4.52	5.03	7.05	6.59	5.72	7.91	7.56	7.23	3.34	11.6	7.96	11.8	10.2	9.85	19.5	20.2	29.1	30.3
Ni	8.03	11.6	28.2	6.84	7.70	10.5	8.39	7.43	10.2	32.5	8.93	8.65	12.4	10.6	5.92	14.0	13.9	13.9	13.5	12.5	59.6	60.6	39.8	42.5
Ga	14.0	17.3	16.7	16.7	15.1	15.5	15.5	15.4	16.9	15.9	16.3	18.8	16.8	16.4	14.1	17.7	15.5	16.9	16.9	17.0	18.6	20.9	24.3	26.5
Pb	35.0	12.3	35.3	33.4	23.7	28.1	30.9	27.4	22.1	29.1	21.2	23.1	23.2	24.9	31.9	21.1	19.3	17.8	19.6	19.2	14.1	14.5	28.2	32.7
Th	11.5	12.9	17.4	16.4	11.8	17.0	14.1	14.7	17.3	14.9	10.1	13.7	10.2	17.5	10.6	19.5	12.3	15.6	11.9	12.4	11.2	11.4	11.5	13.9
U	3.83	4.03	5.26	3.55	4.43	3.61	2.28	2.54	2.13	4.02	3.80	3.17	2.88	4.09	3.31	2.96	2.43	2.48	3.49	3.76	0.90	0.99	1.96	2.19
La	16.1	25.7	23.5	23.8	19.1	25.4	23.2	22.3	42.8	24.0	22.4	31.6	18.7	34.4	16.9	41.7	22.2	31.0	22.2	25.8	53.0	51	33.0	33
Ce	32.0	53.1	49.9	47.9	39.5	51.8	49.7	46.6	85.5	49.2	45.3	64.0	37.9	71.0	35.0	78.0	40.6	61.8	44.8	49.7	103	105	74.4	78
Pr	3.66	5.99	5.70	5.58	4.42	5.99	5.48	5.26	9.26	5.42	4.89	6.97	4.21	7.86	4.18	8.66	4.72	6.80	5.05	5.48	11.5	11.6	7.80	8.1
Nd	14.1	22.1	20.9	20.8	16.8	22.5	20.8	20.3	33.8	20.5	18.5	26.1	16.0	29.1	15.7	30.7	16.9	25.6	19.3	19.9	43.3	42.4	29.0	30.6
Sm	3.11	4.77	4.85	4.83	3.84	5.20	4.72	4.72	6.03	4.40	3.90	5.16	3.58	5.86	3.49	5.80	3.21	5.16	4.14	3.85	6.79	6.63	5.92	5.99
Eu	0.59	0.60	0.52	0.48	0.60	0.70	0.69	0.70	0.93	0.63	0.88	0.94	0.73	0.69	0.43	0.80	0.72	0.74	0.71	0.78	1.79	1.69	1.36	1.35
Gd	2.90	3.67	3.62	3.83	3.37	4.65	4.13	4.35	3.89	3.95	3.14	4.08	3.21	4.22	2.60	4.13	2.45	4.03	3.42	2.89	4.74	4.47	5.27	5.50
Tb	0.58	0.71	0.70	0.72	0.65	0.87	0.82	0.84	0.68	0.74	0.57	0.74	0.64	0.78	0.49	0.80	0.44	0.75	0.63	0.52	0.60	0.59	0.85	0.83
Dy	3.83	4.48	4.45	4.31	4.45	5.76	5.39	5.71	3.95	4.72	3.56	4.66	4.10	4.79	3.08	5.13	2.88	4.84	4.08	3.42	3.26	3.17	4.99	5.06
Ho	0.78	0.84	0.83	0.83	0.91	1.15	1.08	1.17	0.74	0.95	0.68	0.92	0.82	0.92	0.60	1.00	0.57	0.97	0.81	0.67	0.69	0.66	1.01	1.02
Er	2.26	2.44	2.40	2.39	2.72	3.37	3.16	3.41	1.98	2.77	2.03	2.61	2.32	2.58	1.72	2.99	1.75	2.73	2.38	2.01	2.01	2.02	2.98	3.07
Tm	0.33	0.36	0.36	0.35	0.40	0.49	0.47	0.50	0.26	0.40	0.30	0.36	0.33	0.35	0.25	0.43	0.24	0.40	0.35	0.30	0.30	0.29	0.44	0.45
Yb	2.13	2.38	2.37	2.32	2.72	3.24	3.15	3.30	1.67	2.64	2.00	2.37	2.16	2.28	1.61	2.88	1.70	2.62	2.36	2.03	2.03	2.03	3.00	3.09
Lu	0.32	0.33	0.35	0.34	0.39	0.47	0.45	0.48	0.24	0.38	0.29	0.33	0.30	0.33	0.23	0.43	0.25	0.39	0.35	0.31	0.31	0.31	0.45	0.47
Eu_N/Eu^*	0.60	0.44	0.38	0.34	0.51	0.44	0.48	0.47	0.58	0.46	0.76	0.63	0.66	0.43	0.43	0.50	0.78	0.50	0.58	0.71				

RV*: recommended values; MV*: measured values; the values for GBPG-1 from (Jochum et al., 2005), and OU-6 from Potts and Kane (2005).

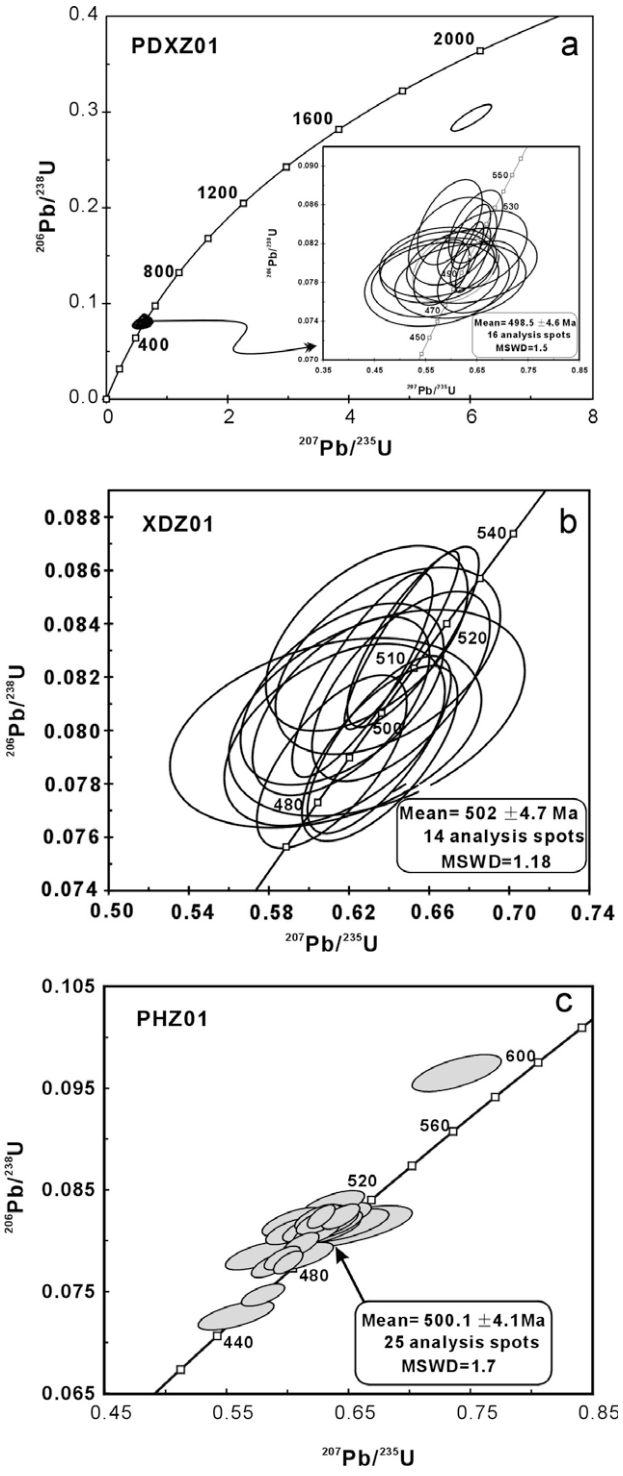

Fig. 3. SHRIMP (a, b) and LA-ICP-MS (c) zircon U–Pb concordia diagrams for monzogranite from the Tengchong–Baoshan Block, Western Yunnan Province.

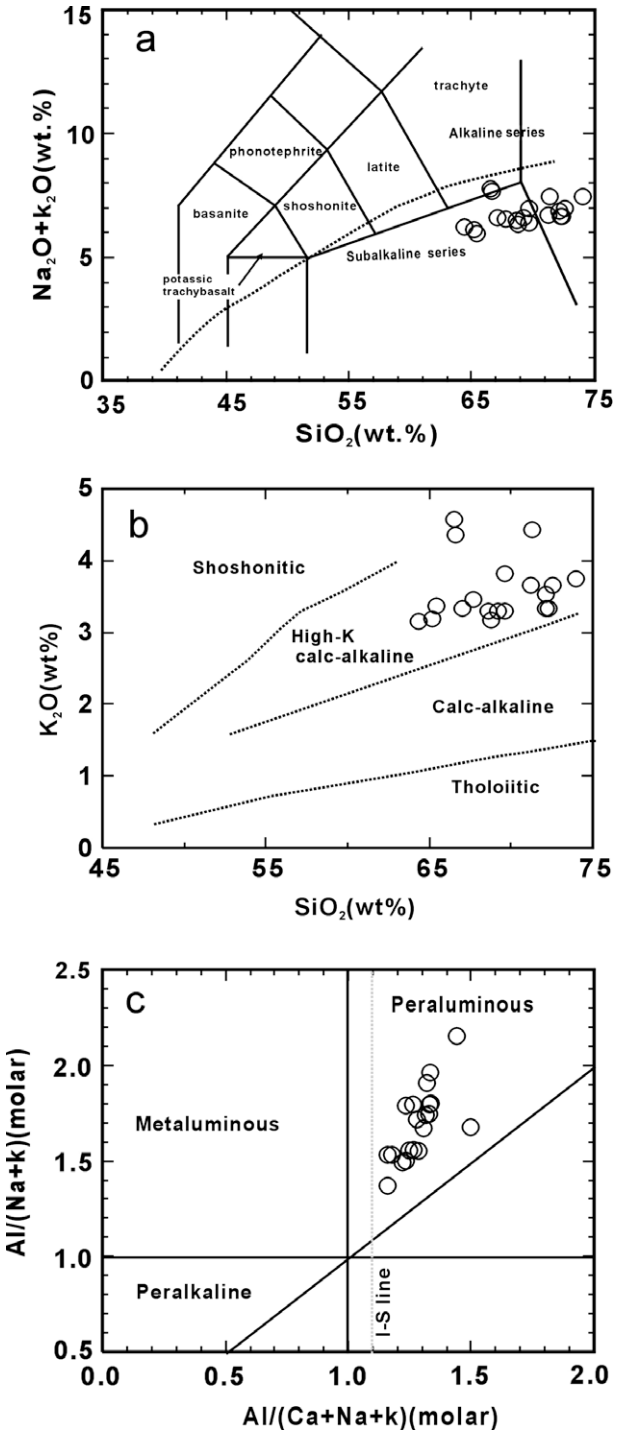

Fig. 4. Classification of the monzogranite on the basis of: (a) the TAS diagram. All of the major element data have been recalculated to 100% on a LOI-free basis (after Middlemost, 1994; Le Maitre, 2002); (b) K_2O *vs.* SiO_2 diagram showing the monzogranite to belong to the high-K, calc-alkaline series (after Roberts and Clemens, 1993); (c) $Al_2O_3/(Na_2O + K_2O)$ molar *vs.* $Al_2O_3/(CaO + Na_2O + K_2O)$ molar plot. Most samples fall within the peraluminous field except for some that fall into either the metaluminous field or straddle the boundary between the two fields.

sistent with crystal fractionation of ferromagnesian minerals, feldspar, Ti–Fe oxides and apatite.

Chondrite-normalised REE patterns of the granitoid rocks invariably are light REE (LREE) enriched. All samples display strong negative Eu-anomalies ($Eu_N/Eu^* = 0.34–0.78$; Table 4; Fig. 7a). These data are comparable with those of the upper crust, but differ from middle–lower crustal signatures (Rudnick and Fountain, 1995). In the primitive mantle-normalised spidergram (Fig. 7b), all samples are enriched in Rb, Th and Pb and depleted in Ba, Nb, Sr, P, Eu, Zr (Hf) and Ti. The (10,000 × Ga)/Al ratios of the granitoids range from 1.8 to 2.3 and, in the Ga/Al *vs.* Zr diagram (Fig. 8; Whalen et al., 1987) all samples fall within the field of I and S-type granites.

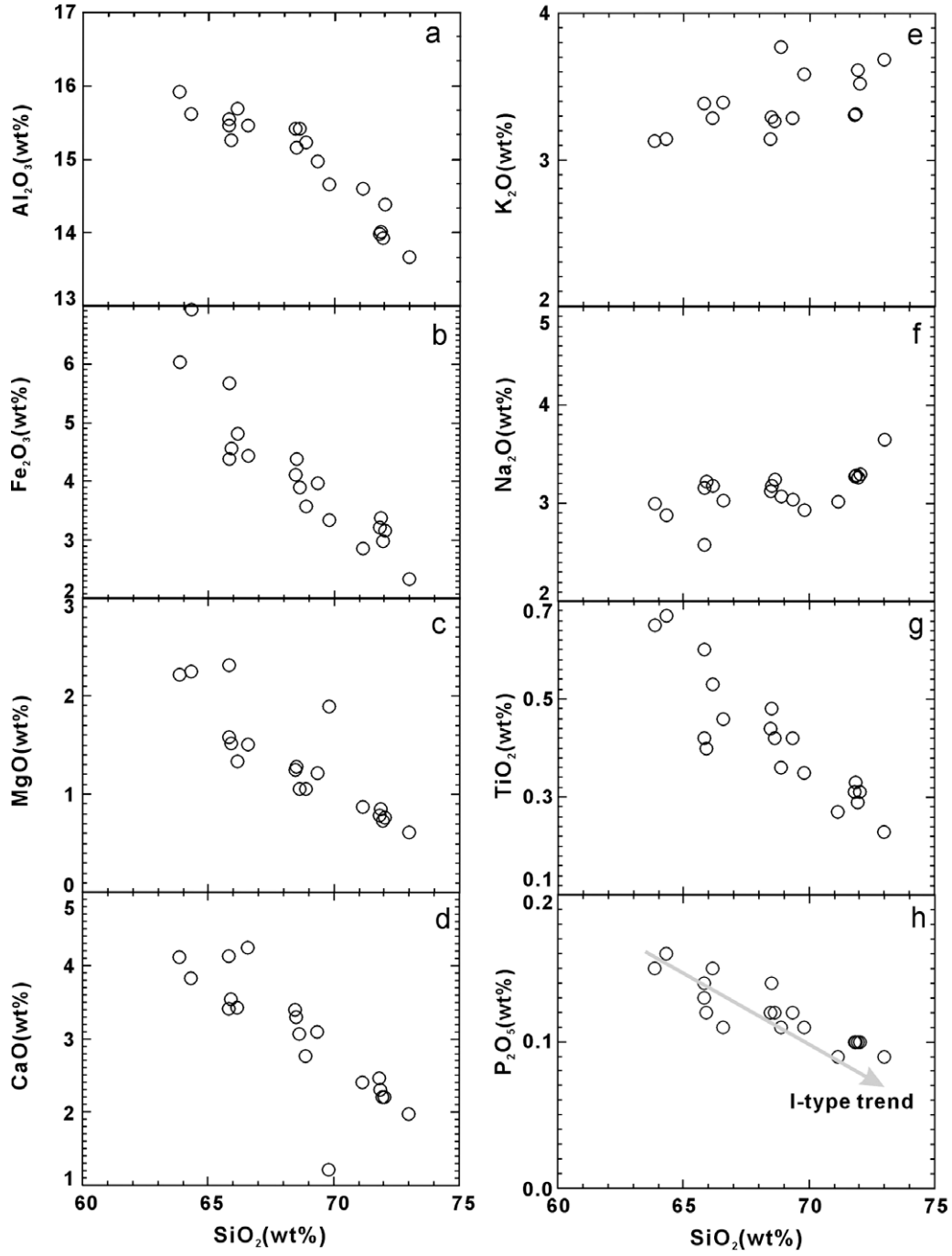

Fig. 5. Chemical variation diagrams for major oxides *vs.* SiO_2 contents for the monzogranite samples from the Tengchong–Baoshan Block, Western Yunnan Province. I-type trend is from Li et al. (2007).

4.3. Nd–Sr isotopes

The Nd and Sr isotopic data were obtained from representative granitoid samples (Table 5). The monzogranite has much lower $(^{143}Nd/^{144}Nd)_i$ (0.511497–0.511512) and $\varepsilon_{Nd}(t)$ values (−9.7 to −9.4) but much higher $(^{87}Sr/^{86}Sr)_i$ ratios (0.7132–0.7144) (Fig. 9a) than Bulk Earth Sr–Nd isotopic compositions (Soler and Rotach-Toulhoat, 1990). This suggests a considerable contribution from an ancient crustal component (e.g., upper crust) in the petrogenesis of these granites. The Nd isotopic compositions are comparable with those of the 490–470 Ma granites ($\varepsilon_{Nd}(t)$ = −8.4 to −9.3) which occur in the southern part of the Tengchong–Baoshan Block (Chen et al., 2004, 2005).

4.4. Zircon Hf isotopes

The determined values for zircon Hf isotopes are given in Table 6. Sixteen spot analyses were obtained for zircon from sample PDXZ01, yielding $\varepsilon_{Hf}(t)$ values of between −13.0 and −10.1, corresponding to T^C_{DM} model ages of between 1610 Ma and 1791 Ma, with an average of $\varepsilon_{Hf}(t) = -11.6 \pm 0.7$ and $T^C_{DM} = 1703 \pm 27$ Ma. Fourteen spot analyses were obtained for zircon from sample

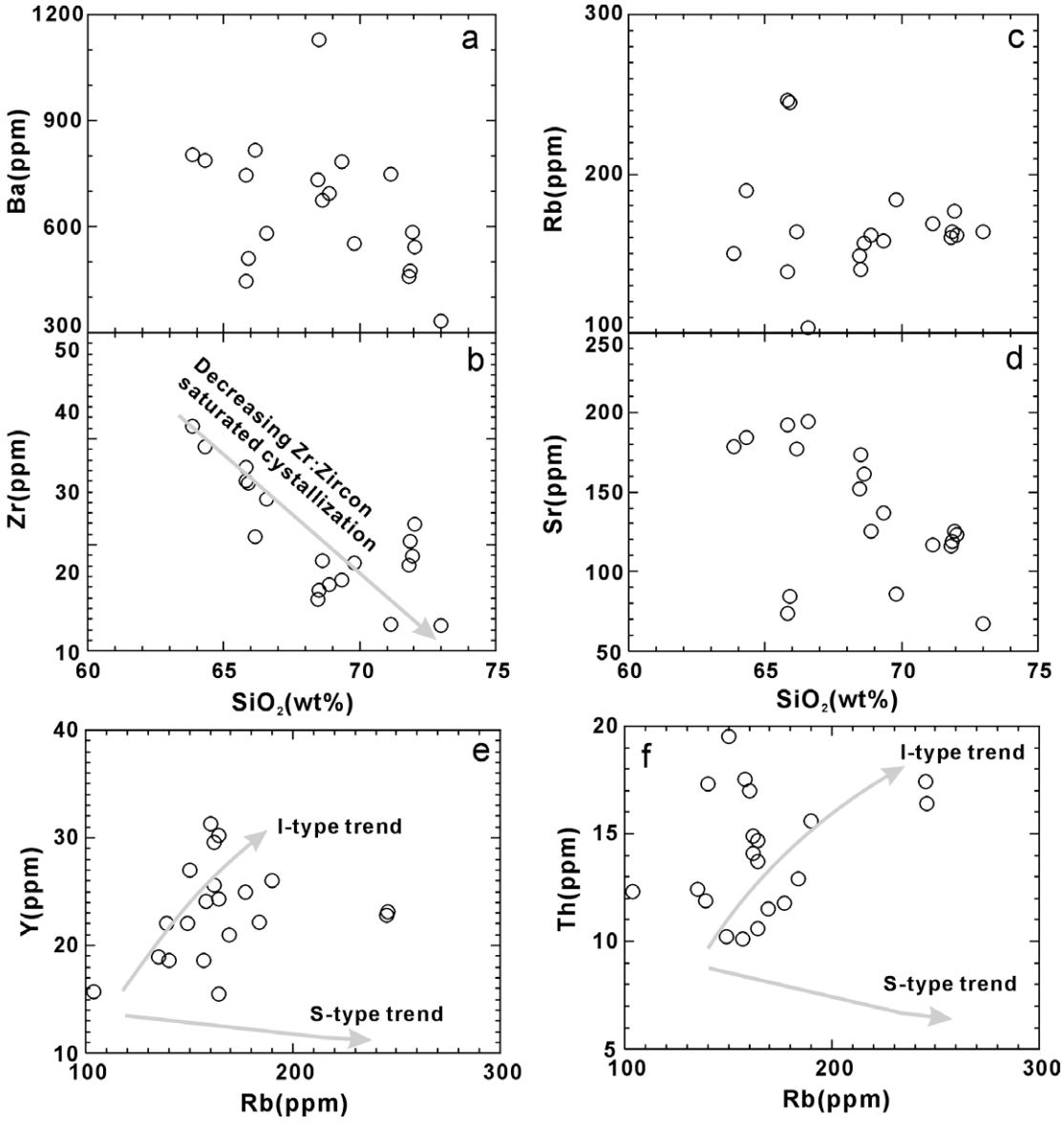

Fig. 6. Variation diagrams (a–d) of selected trace elements *vs.* SiO_2 and (e–f) *vs.* Rb for the monzogranite from the Tengchong–Baoshan Block, Western Yunnan Province. The trend lines are from Li et al. (2007).

XDZ01, giving $\varepsilon_{Hf}(t)$ values of between −10.0 and −12.2, corresponding to T^C_{DM} model ages of between 1603 Ma and 1741 Ma, with a mean $\varepsilon_{Hf}(t) = -11.0 \pm 0.5$ and $T^C_{DM} = 1669 \pm 37$ Ma. Twenty-five spot analyses were made for sample zircon PHZ01. The determined $\varepsilon_{Hf}(t)$ values vary between −10.2 and −13.1, corresponding to T^C_{DM} model ages in the range of 1616–1799 Ma. These spots gave a mean $\varepsilon_{Hf}(t) = -11.6 \pm 1.0$ and $T^C_{DM} = 1708 \pm 50$ Ma. Overall, the Hf isotopic data for zircon from the granitic batholith suggests their derivation from a late Palaeoproterozoic crustal source.

5. Discussion

5.1. Petrogenetic type: S-type, I-type or A-type?

The investigated samples of monzogranite all belong to the high-K series, but have low $Na_2O + K_2O$ values (<7.6%) and 10,000 × Ga/Al ratios (1.8–2.3), distinguishing them from those of the A-type granites (Collins et al., 1982; Whalen et al., 1987). Although the A/CNK values for all of the studied monzogranite samples (Fig. 4c) are comparable with highly felsic, S-type granites that are usually strongly peraluminous, with A/(CNK) values much greater than 1.1 (Chappell, 1999). These rocks exhibit marked reduction in P_2O_5 when SiO_2 contents are high (Fig. 5h). This feature is an important criterion for distinguishing I-type from S-type granites, because apatite reaches saturation in metaluminous and mildly peraluminous magmas (where A/(CNK) < 1.1), but is highly soluble in strongly peraluminous melts (Wolf and London, 1994). The monzogranite also exhibits an increase in Y and Th, as Rb increases, typical of the evolutionary trend for I-type granite (Fig. 6e and f) (Li et al., 2007). Combined with the presence of hornblende, it is evident the studied monzogranite belongs to the high-K, calc-alkaline, I-type, rather than to A- or S-types.

5.2. Fractional crystallisation

The decrease in MgO and Fe_2O_3 during magmatic evolution indicates separation of ferromagnesian minerals (biotite ± hornblende) during crystallisation. Pronounced depletions in Ba, Sr,

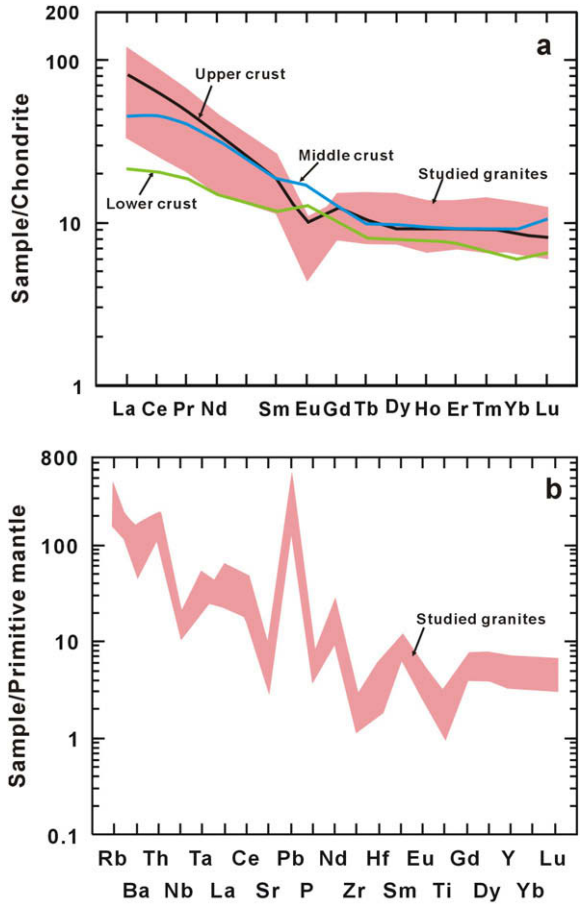

Fig. 7. Chondrite-normalised rare earth element patterns and primitive–mantle-normalised spider diagrams for the monzogranite samples. REE abundances for chondrites and trace element abundance for primitive mantle are after Sun and McDonough (1989). The REE contents for the lower crust, upper crust and middle crust are from Rudnick and Fountain (1995).

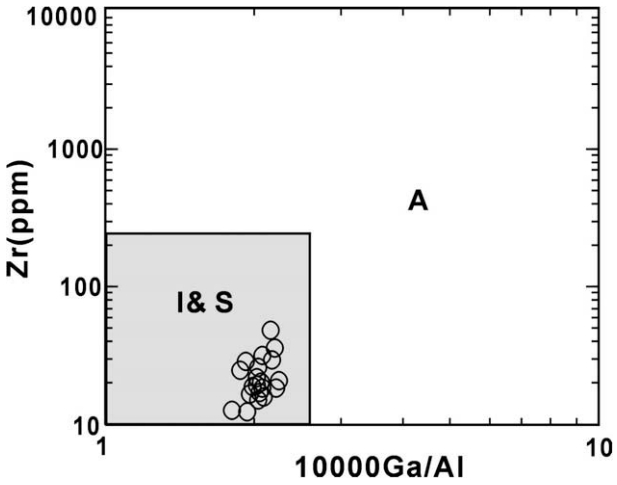

Fig. 8. Monzogranite samples plotted in terms of the Zr *vs.* (10,000 × Ga)/Al diagram of Whalen et al. (1987) indicating their affinity to I- and S-type granitoids.

Nb, P, Ti and Eu (Fig. 7a and b) further demonstrate an advanced process of fractional crystallisation during the formation of these granites. Separation of the Ti-bearing phases (such as ilmenite and titanite) and apatite resulted in depletion in Nb (Ta)–Ti and P, respectively. Strong Ba, Sr and Eu depletion requires extensive fractionation of plagioclase and/or K-feldspar. It can be seen from the Eu_N/Eu^* *vs.* Sr and Ba plots (Fig. 10a and b) that K-feldspar fractionation was more important than plagioclase in controlling Ba content.

The monzogranite exhibits continuously decreasing Zr with increasing SiO_2 (Fig. 6b), which indicates that zircon was saturated in the magma, and that this was also controlled by fractional crystallisation (Li et al., 2007; Zhong et al., 2007). Zircon saturation thermometry (Watson and Harrison, 1983) provides a simple and robust means of estimating magma temperatures from bulk-rock compositions. The calculated zircon saturation temperatures (T_{Zr}) of the granitic rocks were 633–733 °C (Table 2), which represents the crystallisation temperature of the magma.

5.3. The source and petrogenetic model

The high-K, calc-alkaline, I-type monzogranite is characterised by marked negative Nb anomalies and slightly positive Pb anomalies on a multi-element normalised spidergram (Fig. 7b), which is consistent with the involvement of crustal compositions (Rudnick and Fountain, 1995). The granitoid rocks have high initial $^{87}Sr/^{86}Sr$ ratios (0.7132–0.7144) and negative $\varepsilon_{Nd}(t)$ values (−9.7 to −9.4) (Table 5; Fig. 9a), similar to the 490–470 Ma granites originated from upper crust in the southern part of the Baoshan Block (Chen et al., 2004, 2005). This suggests that they may have a common source. Moreover, in combined studies of chondrite-normalised REE diagrams (Fig. 7a), the elevated LREE, some of the trace element contents and ratios, e.g., Th (10.1–19.5 ppm), Pb (17–35 ppm with the exception of one sample), U (2.13–5.26 ppm) and Eu/Eu^* (<1.0) indicate that an upper crustal component, but not the middle–lower crust, is involved in the generation of this monzogranite. For example, rocks derived from upper crustal sources should have relatively higher Th (>10 ppm), Pb (>20 ppm) and U (>2.0 ppm) contents and lower Eu/Eu^* ratios (<1.0), whereas those rocks sourced from middle crust are expected to contain lower Th (<6.0 ppm), Pb (<15 ppm) and U (<1.6 ppm) contents and high Eu/Eu^* ratios (>1.0) (Rudnick and Fountain, 1995). The peraluminous, silica-rich composition of the monzogranite further suggests an important contribution of metasedimentary material among its sources.

The basement to the Tengchong–Baoshan Block is made up of Proterozoic, amphibolite facies, metamorphic rocks (1900–1600 Ma) (Zhai et al., 1990), including terrigenous deposits, continental basalts and intrusive granitoids (Fan and Zhang, 1993; Chen et al., 2005, 2006). The correlation between T^C_{DM} (~1.7 Ga) of the granitoid intrusion and basement rocks, in the Tengchong–Baoshan Block, together with the presence of inherited zircon (1661 Ma), suggest that Proterozoic basement rock has played a key role in the petrogenesis of the studied I-type granitoid. The lack of correlation between the $\varepsilon_{Nd}(t)$ values and Nd concentrations for the monzogranite (Fig. 9b) precludes assimilation and fractional crystallisation (AFC) as a major process during their late evolutionary stages (Zhong et al., 2007), at a shallow-crustal level. Thus, we suggest that the I-type monzogranite was produced by remelting of the Proterozoic basement, although the isotopic characteristics of this basement, at present, are unconstrained.

Calc-alkaline, I-type granitoids of intermediate-to-felsic composition are usually interpreted as being generated either by partial melting of mafic to intermediate igneous sources, or by advanced AFC of mantle-derived basaltic parental magmas (Roberts and Clemens, 1993; Li et al., 2007). However, data on the experimental partial melting of common crustal rocks suggest that high-K, I-type granitoid magma cannot be produced by the latter model, but can only derive from the partial melting of hydrous calc-alkaline to high-K, calc-alkaline, basaltic to intermediate metamorphic rocks, within the crust (Roberts and Clemens, 1993). Experimental stud-

Table 5
Sr–Nd isotopic raios for the granites from Western Yunnan Province.

Sample no.	Age (Ma)	Sm (ppm)	Nd (ppm)	$^{147}Sm/^{144}Nd$	$^{143}Nd/^{144}Nd$	$2S_m$	$(^{143}Nd/^{144}Nd)_i$	$\varepsilon_{Nd}(t)$	Rb(ppm)	Sr(ppm)	$^{87}Rb/^{86}Sr$	$^{87}Sr/^{86}Sr$	$2S_m$	$(^{87}Sr/^{86}Sr)_i$
PH5-7		3.12	14.1	0.1337	0.511940	9	0.511502	−9.6	169	119	4.09	0.74260	10	0.71348
PH5-4	500.1	5.32	21.0	0.1532	0.511998	13	0.511496	−9.7	244	93.2	7.57	0.76796	10	0.71403
PH4-7		4.78	20.4	0.1416	0.511968	8	0.511504	−9.6	165	121	3.85	0.74179	10	0.71439
PH4-6		5.12	21.8	0.1423	0.511975	8	0.511509	−9.5	163	120	3.92	0.74122	12	0.71326
PH3-7		6.13	34.6	0.1105	0.511862	8	0.511500	−9.6	139	175	2.30	0.73002	11	0.71365
PH3-1		5.18	26.4	0.119	0.511902	9	0.511512	−9.4	164	183	2.44	0.73063	10	0.71322
XD-6		3.57	15.9	0.1374	0.511957	10	0.511507	−9.5	146	160	2.63	0.73288	12	0.71415
XD-1	502	3.47	16.2	0.1311	0.511926	8	0.511497	−9.7	169	72.5	6.74	0.76243	10	0.71440
PDX-16		6.01	31.0	0.1155	0.511883	11	0.511505	−9.6	155	184	2.44	0.73072	10	0.71332
PDX-4	498.5	4.40	20.8	0.1278	0.511932	9	0.511515	−9.4	135	202	1.93	0.72696	12	0.71322

Chondrite Uniform Reservoir (CHUR) values ($^{87}Rb/^{86}Sr = 0.0847$, $^{87}Sr/^{86}Sr = 0.7045$, $^{147}Sm/^{144}Nd = 0.1967$ $^{143}Nd/^{144}Nd = 0.512638$) were used for the initial Sr and Nd isotope calculation. $\lambda_{Rb} = 1.42 \times 10^{-11}$ year^{-1} (Steiger and Jäger, 1977); $\lambda_{Sm} = 6.54 \times 10^{-12}$ year^{-1} (Lugmair and Harti, 1978).

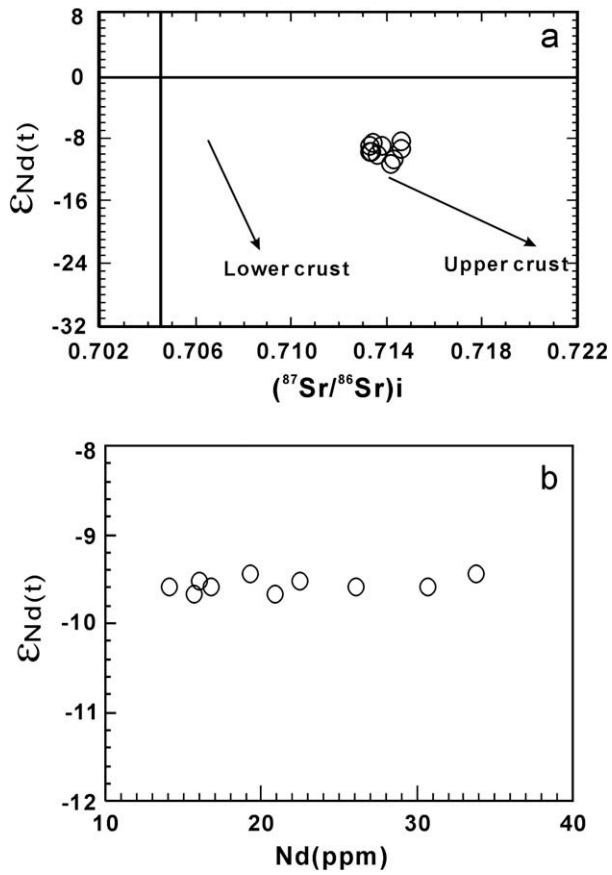

Fig. 9. (a) $\varepsilon_{Nd}(t)$ *vs.* $(^{87}Sr/^{86}Sr)_i$ diagram for the granitoids in the Tengchong–Baoshan Block, Western Yunnan Province. The trends to the lower and upper crust are similar to those of Jahn et al. (1999); (b) Nd *vs.* $\varepsilon_{Nd}(t)$ diagram for the granitoids.

ies further indicate that dehydration melting of tholeiitic amphibolite may produce melts of intermediate to silicic compositions, leaving behind a granulite residue at 8–12 kbar and garnet granulite to eclogite residues at 12–32 kbar (e.g., Rushmer, 1991; Rapp and Watson, 1995). These resultant melts are commonly low in K_2O, with a high Na_2O/K_2O ratio of >1.

High pressure melting is precluded in the formation of the monzogranite in this study because its HREE are not depleted (Fig. 7a), arguing against residual garnet in the source. All samples of monzogranite are high in K_2O, having a Na_2O/K_2O ratio of <1. Accordingly, tholeiitic amphibolite sources are unlikely. Alternatively, using medium-to-high K basaltic compositions as starting materials, Sisson et al. (2005) obtained K-rich melts that have a $Na_2O/K_2O < 1$ at $SiO_2 > 65\%$. On the basis of the above discussion points, we thus prefer this latter model for deciphering the origin of the monzogranite magma in this study.

5.4. Tectonic significance

The late Palaeoproterozoic is an important period for crustal growth in southern China, and ~1.77 Ga, tholeiitic and alkaline amphibolites have been identified in the Cathaysia basement in both NW Fujian and SW Zhejiang (Li, 1997). Contemporaneous crustal growth in Western Yunnan is supported by the present zircon Hf model age data (T^C_{DM}) (~1.7 Ga).

Tectonic discrimination diagrams based on trace elements (such as Rb, Nb, and Y) have been devised for granitoid rocks (Pearce et al., 1984). However, these plots seem to diagnose the environment in which the protoliths were formed, rather than the tectonic settings existing at the time when the granitoid magmas were actually produced (Arculus, 1987; Twist and Harmer, 1987). This suggests that the potentially much older protolith may have formed in a setting very different from that in which the granitoid magma was generated by subsequent partial melting. On plots of Nb *vs.* Y and Rb *vs.* Y + Nb (Fig. 11), the studied monzogranite falls within the fields of volcanic arc granite and syn-collisional granite, indicating that arc-related magmatism likely existed in the Western Yunnan in the Mesoproterozoic. Similarly, arc-related magmatism in the eastern part of Tengchong–Baoshan Block, related to subduction of the palaeo-Tethys ocean (Huang and Chen, 1987; Sun et al., 1991; Chen and Xie, 1994) during the Mesoproterozic, has been suggested by Chen et al. (2006). Subduction of palaeo-Tethys oceanic crust beneath the Western Yunnan continent would have transformed the Tengchong–Baoshan Block into an active continental margin. As a consequence, a back-arc extensional setting may have developed in Tengchong–Baoshan area. This extension, in turn, induced an upwelling of hot asthenosphere, and it was the high heat flow from this asthenospheric mantle and infiltration of slab-derived fluids that triggered intense melting in the lithospheric mantle, producing voluminous basaltic magmas. Subsequently, these mantle-derived magmas ascended along fractures and faults to underplate the upper crust; voluminous granitic magmas were generated by partial melting of the pre-existing, infra-crustal, high-K basaltic metamorphic protoliths (upper crust), heated by the underplated basaltic magmas at 500 Ma. Ascent and coalescence of these Early Palaeozoic granitic magmas resulted in batholith formation throughout the Tengchong–Baoshan Block and adjacent regions (Chen et al., 2004, 2005; this paper; Song et al., 2007). This model is particularly supported by the extensive accretion of back-arc granites in the northwestern margin of the Tengchong–Baoshan Block during Early Palaeozoic times (Chen, 1989). While it is feasible to imagine an

Table 6
Zircon Hf isotopic compositions of the granites from Western Yunnan Province.

Sample	$^{176}Yb/^{177}Hf$(corr)	2σ	$^{176}Lu/^{177}Hf$(corr)	2σ	$^{176}Hf/^{177}Hf$(corr)	2σ	$\varepsilon_{Hf}(t)^*$	T_{DM^*}	$(^{176}Hf/^{177}Hf)_i$	$T^C_{DM^*}$	$f_{Lu/Hf}$
PDXZ01-1	0.035599	0.000272	0.001391	0.000011	0.282131	0.000019	−12.1	1595	0.282118	1740	−0.96
PDXZ01-2	0.035236	0.000264	0.001420	0.000008	0.282190	0.000017	−10.1	1514	0.282177	1610	−0.96
PDXZ01-3	0.028849	0.000581	0.001191	0.000023	0.282172	0.000019	−10.6	1529	0.282161	1645	−0.96
PDXZ01-4	0.032079	0.000600	0.001238	0.000022	0.282127	0.000017	−12.2	1594	0.282116	1745	−0.96
PDXZ01-5	0.031353	0.000544	0.001276	0.000017	0.282159	0.000015	−11.1	1551	0.282147	1676	−0.96
PDXZ01-6	0.037698	0.000706	0.001515	0.000031	0.282126	0.000018	−12.4	1607	0.282112	1754	−0.95
PDXZ01-7	0.032198	0.000661	0.001204	0.000022	0.282135	0.000014	−12.0	1583	0.282123	1729	−0.96
PDXZ01-8	0.038399	0.002259	0.001613	0.000096	0.282156	0.000019	−11.4	1570	0.282141	1690	−0.95
PDXZ01-9	0.040625	0.000478	0.001658	0.000022	0.282137	0.000016	−12.0	1598	0.282122	1732	−0.95
PDXZ01-10	0.033701	0.000587	0.001402	0.000021	0.282166	0.000018	−10.9	1546	0.282153	1663	−0.96
PDXZ01-11	0.034828	0.000320	0.001410	0.000012	0.282107	0.000019	−13.0	1629	0.282094	1791	−0.96
PDXZ01-12	0.010765	0.000064	0.000382	0.000002	0.282133	0.000014	−11.8	1551	0.282129	1715	−0.99
PDXZ01-13	0.042939	0.000773	0.001667	0.000035	0.282131	0.000021	−12.2	1607	0.282116	1743	−0.95
PDXZ01-14	0.032332	0.000199	0.001284	0.000007	0.282167	0.000016	−10.9	1541	0.282155	1660	−0.96
PDXZ01-15	0.023325	0.000341	0.000890	0.000011	0.282184	0.000020	−10.1	1501	0.282176	1613	−0.97
PDXZ01-16	0.047423	0.000250	0.001780	0.000010	0.282132	0.000017	−12.2	1610	0.282116	1746	−0.95
XDZ01-1	0.057356	0.001401	0.002199	0.000053	0.282145	0.000014	−11.9	1610	0.282125	1724	−0.93
XDZ01-2	0.036531	0.000606	0.001427	0.000023	0.282130	0.000021	−12.2	1598	0.282117	1741	−0.96
XDZ01-3	0.042846	0.000495	0.001727	0.000021	0.282153	0.000019	−11.5	1579	0.282136	1697	−0.95
XDZ01-4	0.042890	0.000203	0.001690	0.000006	0.282148	0.000016	−11.6	1584	0.282132	1706	−0.95
XDZ01-5	0.032596	0.001701	0.001251	0.000063	0.282165	0.000019	−10.9	1542	0.282153	1659	−0.96
XDZ01-6	0.035770	0.000143	0.001415	0.000006	0.282192	0.000018	−10.0	1511	0.282179	1603	−0.96
XDZ01-7	0.013630	0.000283	0.000572	0.000011	0.282169	0.000020	−10.5	1510	0.282163	1638	−0.98
XDZ01-8	0.037445	0.000724	0.001436	0.000028	0.282159	0.000019	−11.2	1558	0.282146	1677	−0.96
XDZ01-9	0.035227	0.000256	0.001356	0.000010	0.282157	0.000021	−11.2	1557	0.282144	1679	−0.96
XDZ01-10	0.035655	0.000301	0.001410	0.000012	0.282175	0.000022	−10.6	1535	0.282161	1642	−0.96
XDZ01-11	0.039581	0.000767	0.001537	0.000029	0.282138	0.000019	−11.9	1592	0.282124	1726	−0.95
XDZ01-12	0.019992	0.000189	0.000784	0.000007	0.282175	0.000019	−10.4	1509	0.282168	1627	−0.98
XDZ01-13	0.033393	0.000421	0.001273	0.000017	0.282172	0.000017	−10.6	1533	0.282160	1645	−0.96
XDZ01-14	0.029092	0.000368	0.001117	0.000014	0.282189	0.000018	−10.0	1503	0.282179	1604	−0.97
PHZ01-1	0.040549	0.000394	0.001484	0.000013	0.282106	0.000019	−13.0	1635	0.282092	1793	−0.96
PHZ01-2	0.045015	0.001240	0.001628	0.000046	0.282123	0.000018	−12.5	1618	0.282107	1759	−0.95
PHZ01-3	0.040203	0.000510	0.001530	0.000021	0.282150	0.000016	−11.5	1574	0.282136	1695	−0.95
PHZ01-4	0.060788	0.001178	0.002135	0.000039	0.282109	0.000017	−13.1	1659	0.282089	1799	−0.94
PHZ01-5	0.041981	0.000193	0.001511	0.000004	0.282157	0.000017	−11.2	1564	0.282143	1680	−0.95
PHZ01-6	0.033731	0.000248	0.001242	0.000009	0.282183	0.000018	−10.2	1516	0.282172	1616	−0.96
PHZ01-7	0.038371	0.001066	0.001387	0.000035	0.282158	0.000018	−11.1	1557	0.282145	1674	−0.96
PHZ01-8	0.044749	0.000360	0.001680	0.000013	0.282183	0.000017	−10.4	1535	0.282167	1626	−0.95
PHZ01-9	0.039392	0.000850	0.001439	0.000033	0.282185	0.000018	−10.2	1522	0.282171	1617	−0.96
PHZ01-10	0.043937	0.000119	0.001626	0.000005	0.282146	0.000019	−11.6	1584	0.282131	1706	−0.95
PHZ01-11	0.058775	0.002445	0.002192	0.000090	0.282158	0.000020	−11.4	1591	0.282138	1691	−0.93
PHZ01-12	0.047830	0.000752	0.001818	0.000030	0.282137	0.000018	−12.0	1605	0.282120	1733	−0.95
PHZ01-13	0.042939	0.000773	0.001667	0.000035	0.282131	0.000021	−12.2	1607	0.282116	1743	−0.95
PHZ01-14	0.034111	0.000332	0.001312	0.000014	0.282115	0.000017	−12.7	1615	0.282102	1773	−0.96
PHZ01-15	0.043365	0.000830	0.001621	0.000027	0.282130	0.000017	−12.2	1606	0.282115	1744	−0.95
PHZ01-16	0.055493	0.001645	0.002060	0.000062	0.282115	0.000016	−12.9	1648	0.282096	1788	−0.94
PHZ01-17	0.031833	0.000462	0.001189	0.000015	0.282179	0.000015	−10.4	1520	0.282168	1627	−0.96
PHZ01-18	0.047477	0.000720	0.001807	0.000026	0.282170	0.000018	−10.9	1558	0.282153	1660	−0.95
PHZ01-19	0.039929	0.000411	0.001507	0.000015	0.282181	0.000015	−10.4	1529	0.282167	1629	−0.95
PHZ01-20	0.049927	0.000155	0.001877	0.000009	0.282137	0.000018	−12.1	1608	0.282119	1735	−0.94
PHZ01-21	0.053381	0.002301	0.001989	0.000083	0.282143	0.000020	−11.9	1604	0.282125	1723	−0.94
PHZ01-22	0.041305	0.001171	0.001556	0.000042	0.282127	0.000016	−12.3	1608	0.282113	1750	−0.95
PHZ01-23	0.048845	0.000129	0.001826	0.000006	0.282112	0.000014	−13.0	1642	0.282095	1790	−0.94
PHZ01-24	0.038835	0.001353	0.001429	0.000052	0.282132	0.000018	−12.1	1596	0.282118	1737	−0.96
PHZ01-25	0.028219	0.001283	0.001071	0.000047	0.282183	0.000020	−10.2	1510	0.282173	1617	−0.97

$\varepsilon_{Hf}(t) = 10{,}000\{[(^{176}Hf/^{177}Hf)_s - (^{176}Lu/^{177}Hf)s \cdot (e^{\lambda t} - 1)]/[(^{176}Hf/^{177}Hf)_{CHUR,0} - (^{176}Lu/^{177}Hf)_{CHUR}\,(e^{\lambda t} - 1)] - 1\}$.

$T_{DM^*} = 1/\lambda * \ln\{1 + (^{176}Hf/^{177}Hf)_S - (^{176}Hf/^{177}Hf)_{DM}]/[(^{176}Lu/^{177}Hf)_S - (^{176}Lu/^{177}Hf)_{DM}]\}$.

$T^C_{DM}=1/\lambda * \ln\{1 + [(^{176}Hf/^{177}Hf)_{s,\,t} - (^{176}Hf/^{177}Hf)_{DM,\,t}]/[(^{176}Lu/^{177}Hf)_c - (^{176}Lu/^{177}Hf)_{DM}]\} + t$.

The $^{176}Hf/^{177}Hf$ and $^{176}Lu/^{177}Hf$ ratios of chondrite and depleted mantle at the present are 0.282772 and 0.0332, 0.28325 and 0.0384, respectively (Blichert-Toft and Albarède, 1997; Griffin et al., 2000). $\lambda = 1.867 * 10^{-11}$ a^{-1} (Soderlund et al., 2004). $(^{176}Lu/^{177}Hf)_C = 0.015$, t = crystallization age of zircon.

alternative petrogenetic interpretation that involves monzogranitic magma formation directly from a contemporaneous, ca. 500 Ma, mafic parent that underwent both fractional crystallisation and crustal assimilation. The lack of significant crustal contamination in these granites coupled with experimental evidence to the contrary (e.g., Roberts and Clemens, 1993) makes this an unlikely scenario.

Available radiometric age determinations for the Early Palaeozoic granites from the Tengchong–Baoshan Block (Chen et al., 2004, 2005; this study) and Gongshan Block (Song et al., 2007) range from 470 Ma to 500 Ma (Fig. 1a). This time-frame for magmatism is comparable with the widespread granites that occur throughout the Indian Plate and Himalyan Orogenic Belt (DeCelles et al., 2000; Gehrels et al., 2003; Yin, 2006), micro-segments of the ancient Gondwana supercontinent (Song et al., 2007). These granitoids represent magmatism during the post-Pan-African movement. Granitoids from the period 470–500 Ma, however, are absent from the Yangtze Craton, while Neoproterozoic (~760–850 Ma) granites are widespread (Li et al., 2003a,b; Zheng, 2003). Thus, we propose that the basement of the Tengchong–Baoshan

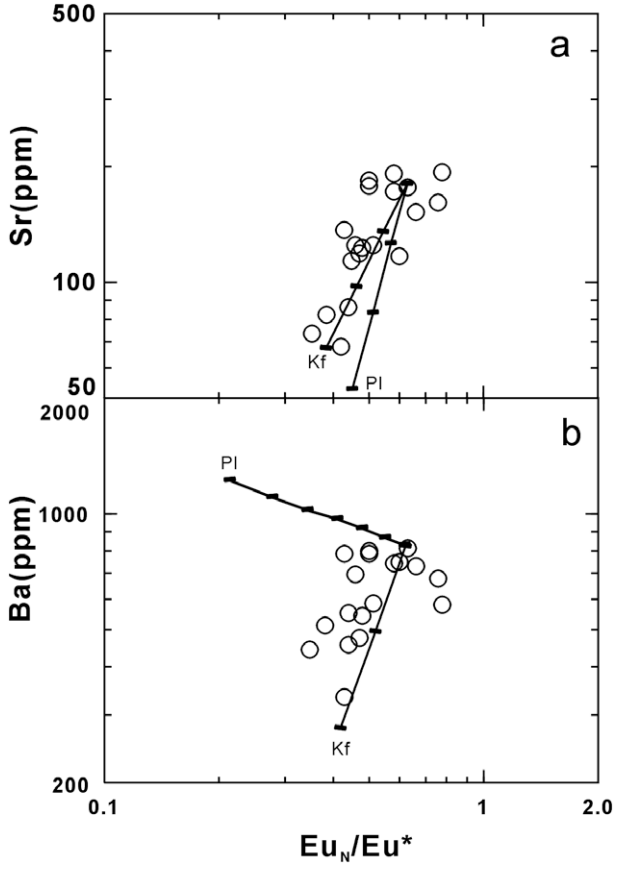

Fig. 10. Plots of: (a) Eu_N/Eu^* *vs.* Sr, and (b) *vs.* Ba for the monzogranite samples. The mineral fractionation vectors, calculated using partition coefficients derive from Philpotts and Schnetzler (1970), Schnetzler and Philpotts (1970) and Bacon and Druitt (1988). The tick marks indicate the percentage of mineral phase removed, in 10% intervals. pl – plagioclase; kf – potassium feldspar.

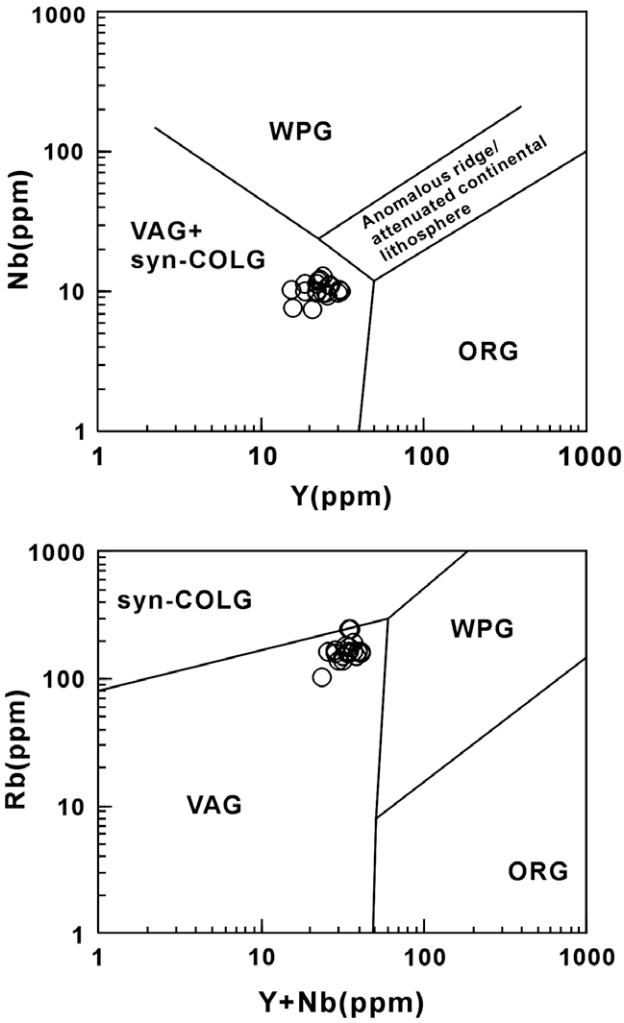

Fig. 11. Trace element discrimination diagrams for the monzogranite samples (Pearce et al., 1984). VAG – volcanic arc granites; ORG – ocean ridge granites; WPG – within-plate granites; SYN-COLG – syn-collisional granites.

and Gongshan blocks are distinct from the Yangtze Craton, but similar to both the Indian Plate and the Himalayan Orogenic Belt, having an affinity with the Gondwana supercontinent. As such, these micro-continents may have formed parts of a single crustal block that broke away from the northern margin of Gondwana, drifting northwards. Other crustal segments, including blocks of Cimmerian (Sengör et al., 1988), Sibumasu and Lhasa (Metcalfe, 1996; Wang et al., 2001; Jin, 2002), along with what is now Australia, India, Antarctica and Sri Lanka also separated from the Gondwana supercontinent in the Late Palaeozoic (Yin and Harrison, 2000).

6. Conclusions

Our geochronological, geochemical and Sr–Nd–Hf isotopic studies of the monzogranite batholith present within Western Yunnan lead us to the following conclusions:

(1) SHRIMP and LA-ICP-MS zircon U–Pb dating gives an intrusion age for the granitoid of ca. 500 Ma (498–502 Ma). The Hf model age (~1.7 Ga) for zircon from the monzogranite suggests magma derivation from a late Palaeoproterozoic crustal source.
(2) Geochemical and Sr–Nd isotopic compositions suggest that the granitoid magmas were generated by partial melting of pre-existing, high-K basaltic metamorphic rocks within the upper crust, which were heated and mixed by underplating basaltic magmas. The resulting I-type granitoid melts underwent extensive fractionation of biotite ± hornblende, ilmenite, titanite, K-feldspar and plagioclase associated with insignificant crustal assimilation during their ascent. Zircon saturation temperatures (T_{Zr}) for the granitoid rocks range between 633 °C and 733 °C, which approximately represents the crystallisation temperature of the magma.
(3) Important crustal growth occurred in the Western Yunnan Province as a result of arc-related magmatism from subduction of the palaeo-tethys ocean.
(4) The Tengchong–Baoshan Block represents an appendant of the former Gondwana supercontinent, and which separated from the supercontinent early in late Palaeozoic, during rifting that also saw separation of what are now Australia, India, Antarctica and Sri Lanka.

Acknowledgements

The authors would like to thank Professor Bor-Ming Jahn, Dr. Anthony Reid and one anonymous reviewer for their constructive reviews on an earlier version of this manuscript. We also thank Dr. L. Jennifer for quick editorial handling of the manuscript. This study was financially supported by the Knowledge innovation project (KZCX2-YW-111-03), Natural Science Foundation of China (40673029, 40773020, 40634020 and 90714010). Prof. Hong

Zhong is acknowledged for his helpful suggestions on this topic. We are grateful to Zhu-Yin Chu, Chao-Feng Li and Xiu-Li Wang for help with the Sr and Nd isotope analysis, Wan-qiang Xie and Yu-Ruo Shi for help with SHRIMP dating, and Dr. Hu-Jun Gong for help in obtaining zircon CL images.

References

Andersen, T., 2002. Correction of common lead in U–Pb analyses that do not report ^{204}Pb. Chemical Geology 192, 59–79.

Arculus, R.J., 1987. The significance of source versus process in the tectonic controls of magma genesis. Journal of Volcanology and Geothermal Research 32, 1–12.

Bacon, C.R., Druitt, T.H., 1988. Compositional evolution of the zoned calc alkaline magma chamber of Mount-Mazama, Crater Lake, Oregon. Contributions to Mineralogy and Petrology 98, 224–256.

Blichert-Toft, J., Albarède, F., 1997. The Lu–Hf geochemistry of chondrites and the evolution of the mantle-crust system. Earth and Planetary Science Letters 148, 243–258.

Chappell, B.W., 1999. Aluminium saturation in I- and S-type granites and the characterization of fractionated haplogranites. Lithos 46, 535–551.

Chappell, B.W., White, A.J.R., 1992. I- and S-type granites in the Lachlan Fold Belt. Transactions of the Royal Society of Edinburgh: Earth Sciences 83, 1–26.

Chen, J.S., 1989. Tectonic settings and lithologic features of the granitoids in west Yunnan Province, China. Yunnan Geology 8, 205–212 (in Chinese with English abstract).

Chen, B., Xie, G., 1994. Evolution of the Tethys in Yunnan and Tibet. Journal of SE Asian Earth Science 9, 349–354.

Chen, F., Siebel, W., Guo, J.H., 2004. Zircon age evidence for Early Paleozoic magmatism in the Baoshan–Tengchong block of the Tethyan Yunnan, China. Geochimica et Cosmochimica Acta, A547.

Chen, F.K., Li, Q.L., Wang, X.L., Li, X.H., 2005. Early Paleozoic magmatism in Baoshan–Tengchong Block of the Tethyan Belt, Yunnan Province. Acta Geoscientica Sinica 26 (Suppl.), 93.

Chen, F.K., Li, Q.L., Wang, X.L., Li, X.H., 2006. Zircon age and Sr–Nd–Hf isotopic composition of migmatite in the eastern Tengchong block, western Yunnan. Acta Petrologica Sinica 22, 439–448.

Collins, W.J., Beams, S.D., White, A.J.R., Chappell, B.W., 1982. Nature and origin A-type granites with particular reference to Southeastern Australia. Contributions to Mineralogy and Petrology 80, 189–200.

Compston, W., Williams, I.S., Kirschvink, J.L., Zhang, Z., Ma, G., 1992. Zircon U–Pb ages from the Early Cambrian time-scale. Journal of the Geological Society, London 149, 171–184.

DeCelles, P.G., Gehrels, G.E., Quade, J., 2000. Tectonic implications of U–Pb zircon ages of the Himalayan Orogenic Belt in Nepal. Science 288, 497–499.

Fan, C.J., Zhang, Y.F., 1993. On the structural pattern of western Yunnan. Yunan Geology 2, 139–147 (in Chinese with English abstract).

Fang, R.S., Fan, J.C., 1993. Some new research on the geological characteristics in the western Yunnan. Geoscience 7 (4), 394–401.

Fang, Z.J., Zhou, Z.C., Lin, M.J., 1990. Some new observations on the geology of western Yunnan. Chinese Science Bulletin 15, 1286–1290.

Gehrels, G.E., DeCelles, P.G., Martin, A., 2003. Initiation of the Himalayan Orogenic as an Early Paleozoic thin-skinned thrust belt. GSA Today 13, 4–9.

Goolaerts, A., Mattielli, N., de Jong, J., Weis, D., Scoates, J.S., 2004. Hf and Lu isotopic reference values for the zircon standard 91500 by MC-ICP-MS. Chemical Geology 206, 1–9.

Govindaraju, G., 1994. Compilation of working values and sample description for 383 geostandards. Geostandards Newsletter 18, 1–158.

Griffin, W.L., Pearson, N.J., Belousova, E., Jackson, S.E., van Achterbergh, E., O'Reilly, S.Y., Shee, S.R., 2000. The Hf isotope composition of cratonic mantle: LAM-MC-ICPMS analysis of zircon megacrysts in kimberlites. Geochimica et Cosmochimica Acta 4, 133–147.

Huang, J.Q., Chen, B.W., 1987. Evolution of the Tethyan Ocean in China and the Neighboring Areas. Geological Press, Beijing. pp. 1–109.

Jahn, B.M., Wu, F.Y., Lo, C.H., Tsai, C.H., 1999. Crust–mantle interaction induced by deep subduction of the continental crust: geochemical and Sr–Nd isotopic evidence from post-collisional mafic–ultramafic intrusions of the northern Dabie complex, central China. Chemical Geology 157, 119–146.

Jin, X.C., 2002. Permo-Carboniferous sequences of Gondwana affinity in southwest China and their paleogeographic implications. Journal of Asian Earth Sciences 20, 633–646.

Jochum, K.P., Nohl, U., Herwig, K., Lammel, E., Stoll, B., Hofmann, A.W., 2005. GeoReM: a new geochemical database for reference materials and isotopic standards. Geostandards Eostandards and Geoanalytical Research 29, 333–338.

Le Maitre, R.W., 2002. Igneous Rocks: A Classification and Glossary of Terms, second ed. Cambridge University Press, Cambridge. 236 pp..

Li, X.H., 1997. Timing of the Cathaysia Block Formation: constraints from SHRIMP U–Pb zircon geochronology. Episodes 30, 188–192.

Li, X.H., Li, Z.X., Ge, W., Zhou, H., Li, W., Liu, Y., Wingate, M.T.D., 2003a. Neoproterozoic granitoids in South China: crustal melting above a mantle plume at ca. 825 Ma? Precambrian Research 122, 45–83.

Li, Z.X., Li, X.H., Kinny, P.D., et al., 2003b. Geochronology of Neoproterozoic syn-rift magmatism in the Yangtze Craton, south China and correlations with other continents: evidence for a mantle superplume that broke up Rodinia. Precambrian Research 122, 85–109.

Li, X.H., Li, Z.X., Li, W.X., Liu, Y., Yuan, C., Wei, G.J., Qi, C.S., 2007. U–Pb zircon, geochemical and Sr–Nd–Hf isotopic constraints on age and origin of Jurassic I- and A-type granites from central Guangdong, SE China: a major igneous event in response to foundering of a subducted flat-slab? Lithos 96, 186–204.

Lizuka, T., Hirata, T., 2005. Improvements of precision and accuracy in in situ Hf isotope microanalysis of zircon using the laser ablation-MC-ICPMS technique. Chemical Geology 220, 121–137.

Ludwig, K.R., 2003. ISOPLOT 3.0: a geochronological toolkit for microsoft excel, Berkeley Geochronology Center. Special publication no. 4.

Lugmair, G.W., Harti, K., 1978. Lunar initial ^{143}Nd/^{144}Nd: differential evolution of the lunar crust and mantle. Earth and Planetary Science Letters 39, 349–357.

Metcalfe, I., 1996. Gondwanaland dispersion, Asian accretion and evolution of eastern Tethys. Australian Journal of Earth Sciences 43, 605–623.

Middlemost, E.A.K., 1994. Naming materials in the magma/igneous rock system. Earth-Science Reviews 74, 193–227.

Pan, G.T., Zhu, D.C., Wang, L.Q., Liao, Z.L., Geng, Q.R., Jiang, X.S., 2004. Bangong lake-Nujiang River suture zone-the northern boundary of Gondwana: evidence from geology and geophysics. Earth Science Frontiers 11, 371–382.

Pearce, J.A., Harris, N.B.W., Tindle, A.G., 1984. Trace element discrimination diagrams for the tectonic interpretation of granitic rocks. Journal of Petrology 25, 956–983.

Philpotts, J.A., Schnetzler, C.C., 1970. Phenocryst-matrix partition coefficients for K, Rb, Sr and Ba, with applications to anorthosite and basalt genesis. Geochimica et Cosmochimica Acta 34, 307–322.

Potts, P.J., Kane, J.S., 2005. International association of geoanalysts certificate of analysis: certified reference material OU-6 (penrhyn slate). Geostandards Eostandards and Geoanalytical Research 29, 233–236.

Qi, L., Hu, J., Grégoire, D.C., 2000. Determination of trace elements in granites by inductively coupled plasma mass spectrometry. Talanta 51, 507–513.

Rapp, R.P., Watson, E.B., 1995. Dehydration melting of metabasalt at 8–32 kbar: implications for continental growth and crust–mantle recycling. Journal of Petrology 36, 891–931.

Roberts, M.P., Clemens, J.D., 1993. Origin of high-potassium, calc-alkaline, I-type granitoids. Geology 21. pp. 825–828.

Rudnick, R.L., Fountain, D.M., 1995. Nature and composition of the continental crust: a lower crustal perspective. Reviews of Geophysics 33, 267–309.

Rushmer, T., 1991. Partial melting of two amphibolites: contrasting experimental results under fluid-absent conditions. Contributions to Mineralogy and Petrology 107, 41–59.

Schnetzler, C.C., Philpotts, J.A., 1970. Partition coefficients of rare-earth elements between igneous matrix material and rock-forming mineral phenocrysts; II. Geochimica et Cosmochimica Acta 34, 331–340.

Sengör, A.M.C., 1984. The Cimmeride Orogenic System and the Tectonics of Eurasia. Geological Society of America, Special Paper 195. Geological Society of America, Boulder, 195 pp.

Sengör, A.M.C., Altiner, D., Cin, A., Ustaomer, T., Hs, K.J., 1988. Origin and assembly of the Tethyside orogenic collage at the expense of Gondwana Land. In: Audley-Charles, M.G., Hallam, A. (Eds.), Gondwana and Tethys. Geol. Soc. Spec. Public. 37, 119–181, Oxford.

Sengör, A.M.C., Cin, A., Rowley, D.B., Nie, S.Y., 1993. Space-time patterns of magmatism along the Tethysides; a preliminary study. Journal of Geology 101, 51–84.

Sisson, T.W., Ratajeski, K., Hankins, W.B., Glazner, A.F., 2005. Voluminous granitic magmas from common basaltic sources. Contributions to Mineralogy and Petrology 148, 635–661.

Soderlund, U., Patchett, P.J., Vervoort, J.D., Isachsen, C.E., 2004. The ^{176}Lu decay constant determined by Lu–Hf and U–Pb isotope systematics of Precambrian mafic intrusions. Earth and Planetary Science Letters 219, 311–324.

Soler, P., Rotach-Toulhoat, N., 1990. Sr–Nd isotope compositions of Cenozoic Granitoids along a Traverse of the Central Peruvian Andes. Geological Journal 25, 351–358.

Song, B., Zhang, Y.H., Wan, Y.S., Jian, P., 2002. Mount making and procedure of the SHRIMP dating. Geological Review 48 (Suppl.), 26–30 (in Chinese).

Song, S.G., Ji, J.Q., Wei, C.J., Su, L., Zheng, Y.D., Song, B., Zhang, L.F., 2007. Early Paleozoic granite in Nujiang River of northwest Yunnan in southwestern China and its tectonic implications. Chinese Science Bulletin 52, 2402–2406.

Steiger, R.H., Jäger, E., 1977. Subcommission on geochronology; convention on the use of decay constants in geochronology and cosmochronology. Earth and Planetary Science Letters 36, 359–362.

Sun, S.S., McDonough, W.F., 1989. Chemical and isotopic systematics of oceanic basalts: implications for mantle composition and processes. In: Saunders, A.D., Norry, M.J. (Eds.), Magmatism in the Ocean Basins. Geological Society Special Publication, London, pp. 313–345.

Sun, S., Li, J.L., Lin, J.L., Wang, Q.C., Chen, H.H., 1991. Indosinides in China and the consumption of Eastern Paleotethys. In: Tectonics and Mountain Building. Academic Press Limited, pp. 363–384.

Twist, D., Harmer, R.E.J., 1987. Geochemistry of contrasting siliceous magmatic suites in the Bushveld complex: genetic aspects and the implications for tectonic discrimination diagrams. Journal of Volcanology and Geothermal Research 32, 83–98.

Ueno, K., 2000. Permian fusulinacean faunas of the Sibumasu and Baoshan blocks, implications for the paleogeographic reconstruction of the Cimmerian continent. Geoscience Journal 4, 160–163.

Von Raumer, J.F., Stampfli, G.M., Borel, G., Bussy, F., 2002. Organization of Pre-Variscan basement areas at the north-Gondwanan margin. International Journal of Earth Sciences 91, 35–52.

Wang, N.W., 1984. The rise of Gondwana research in China and some key problems on paleobiography related to plate tectonics. Bulletin of the Chinese Academy of Geological Sciences 10, 103–115 (in Chinese).

Wang, K.Y., 1996. The tectonic belt in the Sanjiang area of the Yunnan Province and rock units of the Precambrian basements and tectonic evolution along the western margin of the Yangtze block. Geology of Yunnan 15, 138–148 (in Chinese with English abstract).

Wang, X.D., Ueno, K., Mizuno, Y., Sugiyama, T., 2001. Late Palcozoic Faunal, climatic, and geographic changes in the Baoshan Block as a Gondwana-derived continental fragment in southwest China. Palaeogeography Palaeoclimatology Palaeoecology 170, 197–218.

Watson, E.B., Harrison, T.M., 1983. Zircon saturation revisited: temperature and composition effects in a variety of crustal magma types. Earth and Planetary Science Letters 64, 295–304.

Whalen, J.B., Currie, K.L., Chappell, B.W., 1987. A-type granites: geochemical characteristics, discrimination and petrogenesis. Contributions to Mineralogy and Petrology 95, 407–419.

Williams, I.S., 1998. U–Th–Pb geochronology by ion microprobe. In: McKibben, M.A., Shanks III, W.C., Ridley, W.I. (Eds.), Applications of Microanalytical Techniques to Understanding Mineralizing Processes. Rev. Economic Geology 7, 1–35.

Wolf, M.B., London, D., 1994. Apatite dissolution into peraluminous haplogranite melts: an experimental study of solubilities and mechanisms. Geochimica et Cosmochimica Acta 58, 4127–4145.

Woodhead, J., Hergt, J., Shelley, M., Eggins, S., Kemp, R., 2004. Zircon Hf-isotope analysis with an excimer laser, depth profiling, ablation of complex geometries, and concomitant age estimation. Chemical Geology 209, 121–135.

Wopfner, H., 1996. Gondwana origin of the Baoshan and Tengchong terrenes of west Yunnan. In: Hall, R., Blundel, D. (Eds.), Tectonic Evolution of Southeast Asia. Journal of the Geological Society, London. 106, 539–547.

Wu, H., Boulter, C.A., Ke, B., Stow, D.A.V., Wang, Z., 1995. The Changning–Menglian suture zone: a segment of major Cathaysian–Gonwana divides in Southeast Asia. Tectonophysics 242, 267–280.

Wu, F.Y., Yang, Y.H., Xie, L.W., Yang, J.H., Xu, P., 2006. Hf isotopic compositions of the standard zircons and baddeleyites used in U–Pb geochronology. Chemical Geology 234, 105–126.

Xu, P., Wu, F.Y., Xie, L.W., Yang, Y.H., 2004. Hf isotopic compositions of the standard zircons for U–Pb dating. Chinese Science Bulletin 49, 1642–1648.

Yang, Q.J., Xu, Y.G., Huang, X.L., Luo, Z.Y., 2006. Geochronology and geochemistry of granites in the Gaoligong tectonic belt, western Yunnan: tectonic implications. Acta Petrologica Sinica 22 (4), 817–834.

Yin, A., 2006. Cenozoic tectonic evolution of the Himalayan orogenic as constrained by along-strike variation of structural geometry, exhumation history, and foreland sedimentation. Earth Science Review 76, 1–131.

Yin, A., Harrison, T.M., 2000. Geologic evolution of the Himalayan–Tibetan orogen. Annual Reviews in Earth Planetary Science 28, 211–280.

Yuan, H.L., Gao, S., Liu, X.M., Li, H.M., Gunther, D., Wu, F.Y., 2004. Accurate U–Pb age and trace element determinations of zircon by laser ablation—inductively coupled plasma mass spectrometry. Geostandards Newsletter 28, 353–370.

Zhai, M.G., Cong, B.L., Qiao, G.S., Zhang, R.Y., 1990. Sm–Nd and Rb–Sr geochronology of metamorphic rocks from SW Yunnan orogenic zones, China. Acta Petrologica Sinica 6, 1–11.

Zhang, C.H., Wang, Z.Q., Li, J.P., Song, M.S., 1997. Tectonic frame for deformation of the Precambrian metamorphic rocks in the Ximeng ara of the western Yunnan. Regional Geology of China 16, 171–179 (in Chinese with English abstract).

Zhang, H.F., Sun, M., Lu, F.X., Zhou, X.H., Zhou, M., Liu, Y.S., Zhang, G.H., 2001. Geochemical significance of a garnet lherzolite from the Dahongshan kimberlite, Yangtze Craton, southern China. Geochemical Journal 35, 315–331.

Zheng, Y.F., 2003. Neoproterozoic magmatic activity and global change. Chinese Science Bulletin 48, 1639–1656.

Zhong, D.L., 1998. Paleo-Tethyan Orogenic Belt in the Western Parts of the Sichuan and Yunnan Provinces. Science Press, Beijing. pp. 1–231 (in Chinese).

Zhong, H., Zhu, W.G., Chu, Z.Y., He, D.F., Song, X.Y., 2007. Shrimp U–Pb zircon geochronology, geochemistry, and Nd–Sr isotopic study of contrasting granites in the Emeishan large igneous province, SW China. Chemical Geology 236, 112–133.